NASA TECHNICAL NOTE

NASA TN D-7824

NASA TN D-7824

SOME OBSERVATIONS OF THE EFFECTS OF RADIAL DISTORTIONS ON PERFORMANCE OF A TRANSONIC ROTATING BLADE ROW

Donald M. Sandercock and Nelson L. Sanger

Lewis Research Center

Cleveland, Ohio 44135

NATIONAL AERONAUTICS AND SPACE ADMINISTRATION • WASHINGTON, D. C. • DECEMBER 1974

1. Report No.	2. Government Accession No.	3. Recipient's Catalog No.
NASA TN D-7824		

4. Title and Subtitle	5. Report Date
SOME OBSERVATIONS OF THE EFFECTS OF RADIAL DISTORTIONS ON PERFORMANCE OF A TRANSONIC ROTATING BLADE ROW	December 1974
	6. Performing Organization Code
7. Author(s)	8. Performing Organization Report No.
Donald M. Sandercock and Nelson L. Sanger	E-7545
	10. Work Unit No.
9. Performing Organization Name and Address	501-24
Lewis Research Center National Aeronautics and Space Administration Cleveland, Ohio 44135	11. Contract or Grant No.
	13. Type of Report and Period Covered
12. Sponsoring Agency Name and Address	Technical Note
National Aeronautics and Space Administration Washington, D.C. 20546	14. Sponsoring Agency Code

15. Supplementary Notes

16. Abstract

A single rotating blade row was tested with two magnitudes of tip radial distortion and two magnitudes of hub radial distortion imposed on the inlet flow. The rotor was about 50 centimeters (20 in.) in diameter and had a design operating tip speed of approximately 420 meters per second (1380 ft/sec). Overall performance at 60, 80, and 100 percent of equivalent design speed generally showed a decrease (compared to undistorted flow) in rotor stall margin with tip radial distortion but no change, or a slight increase, in rotor stall margin with hub radial distortion. At design speed there was a decrease in rotor overall total pressure ratio and choke flow with all inlet flow distortions. Radial distributions of blade-element parameters are presented for selected operating conditions at design speed.

17. Key Words (Suggested by Author(s))	18. Distribution Statement
Transonic rotating blade row Radial distortion	Unclassified - unlimited Category 01

19. Security Classif. (of this report)	20. Security Classif. (of this page)	21. No. of Pages	22. Price*
Unclassified	Unclassified	49	$3.75

* For sale by the National Technical Information Service, Springfield, Virginia 22151

SOME OBSERVATIONS OF THE EFFECTS OF RADIAL DISTORTIONS ON PERFORMANCE OF A TRANSONIC ROTATING BLADE ROW

by Donald M. Sandercock and Nelson L. Sanger

Lewis Research Center

SUMMARY

A single rotating blade row was tested with two magnitudes of tip radial distortion and two magnitudes of hub radial distortion imposed on the inlet flow. The rotor was approximately 50 centimeters (20 in.) in diameter and had a design operating tip speed of approximately 420 meters per second (1380 ft/sec). Overall performance is presented at 60, 80, and 100 percent of equivalent design speed. Blade-element parameters are compared at selected operating conditions at 100 percent of design speed only.

With tip radial distortion a decrease in rotor stall margin was observed at all speeds. With hub radial distortion there was generally no change or a slight increase in rotor stall margin. With both types of distortion there was a decrease in the choke flow rate at 100 percent of design speed.

Radial distributions of blade-element parameters (100 percent of design speed) showed the following: At a given flow rate the decrease in overall total pressure with distortion was related to the reduced inlet total pressure in the distorted flow region and the unloading of the blade elements in the undistorted flow region. Rotor stall was coincident with the occurrence of critical flow conditions in the blade tip region. For each type of inlet flow (i.e., distorted or undistorted) the tip critical flows occurred at a different overall flow rate. The different maximum, or choked, flow rates were probably associated with the more peaked inlet velocity distributions resulting from the inlet distortions. However, criteria for estimating the choking flows were not apparent from the data.

Over the design speed operating range with inlet distortion the hub and tip blade elements operated in significantly different (from undistorted flow) ranges of incidence angle and axial velocity ratio for approximately the same blade loading (diffusion factor) ranges.

INTRODUCTION

In the design of most fans and compressors the stagnation conditions (pressure and temperature) of the flow entering the first stage are usually assumed to be uniform over essentially the entire face of the inlet blade row. However, it is recognized that, because of engine inlet geometry, aircraft maneuvering, wind gusts, inlet shock patterns, and other interactions, the compressor will probably operate with the inlet stagnation conditions distorted (from the assumed uniformity) to some extent and magnitude. Thus, for any new design, it is desirable to have some knowledge of the response of the fan or compressor to a distorted inlet flow. Of particular interest is any degradation in compressor performance (pressure ratio, flow, and stable operating range) resulting from the distorted inlet flow.

In experimental studies carried out in compressor test facilities the inlet total pressure is generally distorted by means of screens located upstream of the inlet stage. Usually, simple patterns of distortion (a tip radial, a hub radial, and a circumferential) are introduced into the inlet flow, and the response of the compressor to each is studied individually. In this study, flows with radial distortion patterns were investigated. A tip (or hub) radial distortion pattern extends in an annular section about the circumference. The bounding radii of the annular section are usually selected to make the distorted flow area some desired percentage of the total flow area. The magnitude of the distortion is controlled by the screen porosity.

As a part of the overall research program on fans and compressors carried out at the Lewis Research Center, the response of a compressor to selected inlet flow distortion patterns was measured. In this report the response of a single rotating transonic blade row to hub radial and tip radial inlet flow distortion is presented and discussed. Test data were taken at two magnitudes of tip radial distortion and two magnitudes of hub radial distortion, and detailed surveys of flow conditions were made so that both overall performance and radial distributions of blade-element parameters were used in the evaluation. The effects of inlet radial distortion on rotor operation are discussed primarily in terms of deviations from the base-line performance which was obtained with undistorted inlet flow.

The work reported herein was performed in the U.S. customary system of units. Conversion to International System of Units (SI) was done for reporting purposes only.

APPARATUS AND PROCEDURE

Rotor

The design of the rotor used in this investigation (designated as rotor 5) is described in detail in reference 1. Design overall parameters are listed in table I. Aerodynamic design parameters and blade geometry are presented in detail in reference 1. All symbols are defined in appendix A. The rotor was approximately 50 centimeters (20 in.) in diameter at the blade leading edge and operated at a blade tip speed of about 420 meters per second (1380 ft/sec). In the higher-relative-Mach-number tip regions (outer 20 percent of span), multiple-circular-arc blade shapes were utilized. At other spanwise locations (inner 80 percent of span) a double-circular-arc blade shape was used. Part-span dampers were mounted on the blades at approximately 43 percent of the span from the rotor tip. Additional design details may be obtained from reference 1. The rotor is shown in figure 1.

Test Facility

The test facility is described by the schematic diagram shown in figure 2. For the tests reported herein the atmospheric inlet and altitude exhaust options in the system were used. For these distortion tests the inlet annulus was lengthened (compared with that used for tests reported in ref. 1) in order that the distortion screens could be located a distance of approximately 32 centimeters (12.6 in.) upstream of the compressor rotor. A line diagram of the compressor test section including the screen location, passage curvature across the test rotor, and location of the rotor inlet and outlet flow measuring stations is shown in figure 3.

Instrumentation

The axial locations of survey instrumentation are shown in figure 3. The type of probe used to obtain the survey data is shown in figure 4 and reported in reference 2. This double-barrel probe has demonstrated ability to measure accurate values of total temperature, total pressure, and flow angle. For these distortion tests, where it was thought desirable to obtain all measurements at the same location, static pressures were obtained by averaging the pressures measured from the taps on the two sides of the 60° wedge and by utilizing calibration curves relating these readings with true static pressures. The calibration curves showed that relatively high corrections had to be applied to the probe measurements in order to determine true static pressures. A typical

calibration curve (taken from ref. 2) is shown in figure 5. Note the large correction factor and the sensitivity of the correction to Mach number in the range of a $0.6 < M < 1.0$. This is in the range of flow Mach numbers entering and leaving this rotor at design speed. However, emphasis herein is placed on the change in flow conditions (from undistorted inlet flow conditions) caused by inlet flow distortions rather than on the absolute value of any single flow parameter.

Test and Calculation Procedures

Compressor test data were taken over a range of weight flows from maximum flow to stall at blade speeds of 60, 80, and 100 percent of equivalent design speed. A survey consisted of measurements at 11 radial positions. Compressor stall was identified by a rapid fluctuation in the signal from a hot-film gage located at the rotor inlet. Fluctuations in compressor discharge pressure and blade stress also were observed. The data points nearest stall for each speed at which surveys were taken are within 0.45 kilogram per second (1 lbm/sec) of the weight flow recorded at stall.

Measured outlet total temperatures and total pressures were corrected for Mach number and streamline slope according to the calibrations given in reference 1. Static pressure was also corrected for Mach number and streamline slope as previously noted.

Blade-element and overall performance parameters were calculated in accordance with the equations defined in appendix B. All parameters presented herein are based on data calculated to lie on blade leading and trailing edges. The translation of flow parameters from the measuring stations to the blade leading and trailing edges were made by using the following assumptions: (1) the actual radii and slopes of the streamlines correspond to those of the design streamlines; (2) the total pressure, total temperature, and angular momentum of flow along any given streamline are constant between the measuring station and the blade edge; (3) the ratio of the weight flow per unit area (static density times axial velocity) at the measuring station to the weight flow per unit area at the blade edge along any given streamline is equal to the ratio calculated from the flow parameters in design.

Distortion Screens

The radial distortion screens used in this investigation were located in the inlet flow path 32 centimeters upstream of the rotor, as shown in figure 3. The radial screens were sized to cover 40 percent of the flow area in the hub or tip region. Different porosities were chosen to provide different magnitudes of distortion as defined by the distortion parameter

$$(\text{Distortion parameter})_{\text{Radial}} = \frac{P_{max} - P_{min}}{P_{max}}$$

Flow measurements at the rotor inlet show that the inlet flow distortion was higher in the tip region than in the hub region. One reason for this is the flow path just upstream of the screen location. For a given weight flow and a screen with the same porosity, the accelerating flows around the bellmouth inlet which enter the screen in the tip region would have a higher dynamic head $\left(\frac{1}{2}\rho V^2\right)$. Consequently, the total pressure drop (and distortion parameter) would be higher in the tip region. In addition, a local radial gradient of velocity close to the outer wall could result in a radially varying degree of distortion.

In this investigation the radial extent and magnitude of inlet pressure distortion at the compressor inlet were accepted as measured, and the performance was recorded. Experience does point out the probability that some iteration of the screen extent and porosity will be required if a specific distortion pattern at the rotor inlet is desired.

RESULTS AND DISCUSSION

The data presented herein were measured from the same rotor whose performance is reported in reference 1. There are some obvious differences between the performance and flow parameters presented in reference 1 and the undistorted inlet flow parameters reported herein. No attempt will be made to analyze these differences other than to point out two principal changes that were present in this investigation as compared with that of reference 1:

(1) The inlet flow annulus was lengthened to permit the distortion screens to be located about 32 centimeters (12.6 in.) upstream of the rotor.

(2) Static pressures used herein were obtained from static pressure taps on a 60° wedge probe as compared with the $7\frac{1}{2}^\circ$ wedge probes used in reference 1. Consequently, larger correction factors were needed in this investigation.

All the data presented herein were obtained from the same rotating blade row operating in the same test facility and using the same measurement system. Emphasis is placed on changes in performance and flow parameters from base-line conditions as the various radial distortion patterns were imposed on the rotor inlet flow. Base-line performance is that obtained with undistorted inlet flow.

It should also be recognized throughout that the results were obtained from a single rotating blade row. When a stator row is added to form a complete stage, some modifications to the performance and trends noted may be expected.

Overall performance with various types of inlet flow distortions at three constant corrected speeds (60, 80, and 100 percent of equivalent design speed) were first examined. From these data, certain operating conditions were selected for further analysis by using detailed radial distributions of blade-element parameters.

Overall Performance

The overall performance of this rotor with various inlet flow distortions is presented in figure 6. Mass-averaged pressure ratio and efficiency are presented as functions of corrected weight flow. Constant-speed operating characteristics are defined at corrected speeds of 60, 80, and 100 percent of design speed. At corrected speeds of 70 and 90 percent of design, only near-stall operating points are presented. Design tip speed at the rotor inlet was approximately 420 meters per second (1380 ft/sec). On all plots the base-line performance for undistorted flow is included for comparison.

The general effects of radial distortion (as compared with undistorted inlet flow) on the pressure ratio, efficiency, and stable operating range of this rotor are obvious from figure 6. The largest effects occurred at design speeds, where the magnitude of the distortion was the highest. Lesser effects of distortion are observed at speeds lower than design, where distortion was reduced.

A preferred index for indicating the magnitude of the inlet distortion has not been generally accepted. As a measure of the distortion, two relatively simple distortion parameters, defined as

$$\frac{P_{max} - P_{min}}{P_{max}} \tag{1}$$

and

$$\frac{P_{av} - P_{min}}{P_{av}} \tag{2}$$

are presented herein. Average values for the distortion parameter defined by expression (1) at design speed are given on the figures for identification. Since the same distortion screens were used at all operating conditions, these values will vary directly with weight flow. Values for both distortion parameters over a range of weight flows are presented in table II.

In order to aid in assessing the performance changes with inlet flow distortion and, in particular, the quantitative changes in stall margin, a fan operating line was imposed on the plots. The relatively simple flow model used to construct the operating line assumes that the exit flow nozzle expands to ambient pressure and there is no loss in total pressure from the fan rotor outlet to the nozzle outlet. Thus, the nozzle expansion ratio (and consequently a nozzle exit Mach number) can be related to the inverse of the fan rotor total pressure ratio. With inlet distortion the operating line differed from the undistorted flow operating line, tending to move the distorted operating line closer to the stall line. The exit nozzle was sized so that the operating line passes through the design point and the following operating point on the undistorted inlet flow characteristic:

$$N/\sqrt{\theta} = 100 \text{ percent of design speed}$$

$$P_2/P_1 = 1.660$$

$$W\sqrt{\theta}/\delta = 65.47$$

The most obvious result based on this selected operating line is that for the largest tip radial distortion the fan rotor would have no stall margin at speeds of 80 percent of the design operating speed and below.

Of particular interest is the effect of an inlet flow distortion on the stalling characteristics of the fan. A well-defined method for quantitatively evaluating these effects has not been established. Herein the effects of distortion on the stall line are shown in terms of stall pressure ratio according to

$$\left[\frac{(PR)_{s,\text{distorted}} - (PR)_{s,\text{undistorted}}}{(PR)_{s,\text{undistorted}}}\right]_{N/\sqrt{\theta} = \text{Constant}} \tag{3}$$

The values from the computation (expression (3)) are summarized in table III. Table III shows the effects of inlet distortion on stall pressure ratio but does not indicate the complete movement of the stall line (fig. 6) since the changes in flow range are not accounted for. Stall pressure ratios with and without distortion were also compared at a constant weight flow. Stall pressure ratios with distortion are listed in table III (from fig. 6). Stall pressure ratios for undistorted flow at the same weight flow were also obtained from figure 6. The stall pressure ratio values were applied to form a parameter of the same form as expression (3) but at a constant weight flow. Parameter values are listed in table III. These parameter values provided a somewhat more consistent description of the movement of the stall line as inlet flow distortion was applied.

The overall performances for all test conditions at 100 percent of design speed are compared in figure 7. This figure allows a more complete comparison of the effects of inlet flow distortion on stable operating range, maximum flow, and maximum efficiency. From this figure the following three operating conditions were selected for presentation of more detailed radial distributions of blade-element parameters:

(1) A common corrected weight flow of approximately 96 percent of design flow

(2) Near-stall operation for all flow conditions

(3) At choke flow for all flow conditions

Comparisons of detailed performance and flow parameters at these three flow conditions are presented in the following sections.

Operation at the Same Flow

The radial distributions shown in figure 8 illustrate how a radial distortion to the inlet flow forces the individual blade elements along the blade span to operate, as compared with undistorted inlet flow operation. The flow entering the blade row in all cases was essentially the same at a corrected weight flow of 96 percent of design flow (an operating point at which blade-element data with undistorted as well both types of radial distortion were directly available). The discussion is directed primarily to changes in flow conditions from the undistorted inlet distributions as a radial distortion was applied. All data shown are values occurring on the blade leading and trailing edges. Not every parameter plotted in figure 8 is discussed individually. Rather the parameters are used as needed to make various flow or performance comparisons. Those parameters not used in the discussion are included to permit calculation of velocity diagrams and other desired flow parameters. The rotor blade row had a part-span damper located at 43 percent of span from the rotor tip. The effects of the damper on the flow in that region are evident in the radial distributions of parameters at the rotor exit.

The radial distribution of inlet total pressure P_1 shows the actual distortion to P_1 as measured at the blade inlet. The P_1 values have been corrected so that the mass-averaged level of P_1 is 10.14 N/cm^2 (14.7 lbf/in.^{2}) in all cases. The plots show that the tip radial screen produced a distortion to inlet total pressure P_1 which varied with radius and covered at least 52 percent of the inlet flow area (based on the portion of the blade span over which P_1 is below 10.14 N/cm^2). The minimum and maximum inlet total pressures P_1 of 8.48 and 10.89 N/cm^2 (12.3 and 15.8 lbf/in.^{2}) were used to compute the following distortion indices:

$$\frac{P_{max} - P_{min}}{P_{max}} = 0.222$$

$$\frac{P_{av} - P_{min}}{P_{av}} = 0.163$$

Similar calculations of flow with the hub radial screen show that the distorted flow covered an area of approximately 21 percent of the total inlet flow area, and the following distortion indices were calculated:

$$\frac{P_{max} - P_{min}}{P_{max}} = 0.116$$

$$\frac{P_{av} - P_{min}}{P_{av}} = 0.088$$

The radial distributions of axial air velocity $V_{z,1}$ at the rotor inlet (fig. 8(c)) indicate the shifting of flow away from the distorted flow area and into the undistorted flow areas. With undistorted inlet flow the curvature of the passage inner and outer walls at the blade inlet were such that the peak throughflow velocity $V_{z,1}$ occurred near the midspan of the blade. Both the hub and tip radial distortions tend to amplify this peak value. Both the $V_{z,1}$ and the resulting distribution of incidence angle with the blade suction surface i_{ss} (fig. 8(b)) had a tendency to affect the radial variation of blade loading. The increased i_{ss} values in the distorted flow regions would be expected to increase the blade loading (above the undistorted inlet flow level), while the loading in the undistorted flow regions would be expected to decrease.

The total temperature ratio T_2/T_1 distributions (fig. 8(d)) indicate that with either type of radial distortion the energy addition was lower at all radii than that achieved with undistorted inlet flow. This, in turn, indicates that the increased loading expected in the distorted flow regions from the i_{ss} plots was not realized. The distribution of the diffusion factor D, a blade loading parameter, verifies this. A possible reason for this lack of increased loading is best explained by the following stepwise flow procedure:

(1) At the blade inlet the high i_{ss} (tendency to increase loading) flow occurred in a low P_1 region, while the low i_{ss} (tendency to decrease loading) flow occurred in a high P_1 region.

(2) As a result of step 1 the general level of P_2 at the blade row outlet was reduced from that achieved with undistorted inlet flow.

(3) In order to pass the same total mass flow, the general lower-density-level flow required an increase in the average level of axial velocity $V_{z,2}$ (fig. 8(k)). This increased $V_{z,2}$ tended, in turn, to reduce the energy addition and blade loading.

The plots of figure 8, of course, reflect this flow process in an equilibrium state - both axially and radially.

The radial distributions of total pressure ratio P_2/P_1 (fig. 8(f)) reflect the effects of both the energy addition T_2/T_1 (fig. 8(d)) and the loss coefficient $\bar{\omega}$ (fig. 8(g)). Measured P_2/P_1 values slightly exceeded the undistorted inlet values in the tip region (0 to 15 percent of span) with tip radial distortion and in the hub region (85 to 100 percent of span) with hub radial distortion. However, the radial distributions of absolute outlet total pressure P_2 (fig. 8(e)) show the level of P_2 with distortion to be well below the level with the undistorted inlet at all radii.

A general comparison of the outlet P_2 distributions with the inlet P_1 distributions indicates that the radial distortion of total pressure was attenuated somewhat across the rotor. For the maximum and minimum values of P_2 shown on the plots, the following distortion indices were calculated at the rotor outlet:

(1) With tip radial distortion

$$\frac{P_{max} - P_{min}}{P_{max}} = \frac{16.4 - 14.9}{16.4} = 0.092$$

(2) With hub radial distortion

$$\frac{P_{max} - P_{min}}{P_{max}} = \frac{17.9 - 16.0}{17.9} = 0.106$$

In terms of distortion parameter, comparison of these values with similarly computed values at the rotor inlet (0.222 and 0.116, respectively) shows a significant attenuation of tip radial distortion and a very small attenuation of hub radial distortion.

In general, the response of an axial-flow rotor to a radial inlet distortion would be toward attenuation of the distortion. In the low-inlet-pressure (and low flow) regions the blade-element loading tends to be increased while, conversely, in the higher-inlet-pressure (and high flow) regions the blade-element loading tends to be decreased. Thus, the level of P_2 tends to equalize at the rotor outlet. The radial distribution of outlet total pressure is also affected by the relatively greater response (in terms of energy input) of tip elements to a flow or incidence angle change, as compared with hub elements, for a rotor row with a low hub- to tip-radius ratio. This reasoning assumes that a critical flow condition is not reached in any blade element or that the hub blade elements do not turn the flow past the axial direction.

Inherent in the data measuring and data reduction processes is the assumption that streamlines under all operating conditions pass through the specified inlet and outlet

radial locations at which measurements are taken. Thus, a measured flow change is always related to known (and the same) blade section geometry. The streamline locations and associated blade geometry are given by the design calculations presented in reference 1. It is recognized that the streamline locations will vary with operating condition and with inlet flow distortion. However, for simplicity, the data shown are those taken and processed under the assumption of constant streamlines.

In order to aid in estimating streamline locations, the ρV_z distributions at the inlet and outlet measuring stations (for the three operating conditions) were integrated and plotted against span as a percent of the total integrated flow. These radial variations, shown in figures 9(a) to (c), allow some estimation of actual streamline (equal percentages of total flow) location. In figure 9(d) the location of selected streamlines at the blade inlet and outlet measuring stations with and without distortion are compared. A linear variation across the blade row was assumed. In general, the plots indicate that the streamlines did not vary appreciably (from the undistorted inlet flow location) when the lighter hub radial distortion was applied but that they did vary a significant amount when the heavier tip radial distortion was applied. For the case of tip radial distortion shown in figure 9(c), sample calculations indicate that the tip streamline flow diffusion factor, axial velocity ratio, and loss coefficient varied less than about 10 percent depending on whether measurements taken on the actual streamline (fig. 9(d)) or on the assumed design streamline were used. This relatively small change would indicate that the radial distributions of most parameters shown (for design streamlines) would not vary significantly if actual streamline values were computed. However, when estimating local flow conditions within the blade row, use of actual streamlines would be preferable.

Operation at Near-Stall Conditions

The radial distributions of blade-element parameters at near-stall operation for the undistorted inlet flow and both levels and types of inlet flow distortion are shown in figure 10. As noted in figure 6, stall occurred at a different flow rate for each type of inlet flow condition. Attention is directed herein to the similarities in flow conditions during operation close to a stalling condition.

Examination of the plots of figure 10 indicates several obvious similarities in near-stall operation:

(1) For all cases, the highest values of T_2 (or ΔT, or T_2/T_1 since T_1 was constant radially) and D, which are both measures of blade loading for this given rotor and blade speed, occurred across the blade element closest to the blade tip. This indicates that a stall condition was initiated when this tip element (or tip region) reached a critical flow condition. Note that when the tip element reached a given level of T_2 or D, blade

stall was imminent even though the other blade elements were operating at widely different levels of blade loading.

(2) For all cases, except the one with the highest level of inlet tip radial distortion, the diffusion factor at the 7-percent-of-span element at near-stall conditions was approximately 0.63 and T_2 was approximately 359 K (ΔT = 88.5 K for T_1 = 270.5 K).

This information aids in explaining the differences in stalling weight flow (as a radial distortion was applied) shown by the overall performance (fig. 6). When a tip radial distortion was applied, the blade tip loading tended to increase and thus reached the critical flow condition at a higher flow rate than with undistorted inlet flow. Conversely, a hub radial distortion tended to unload the blade tip elements and the critical flow condition was not encountered (in the tip) until a lower weight flow was reached. This explanation is relatively simple as applied to this rotating blade row, where it can be reasonably established that the blade tip region always reached a critical flow condition before the other spanwise blade elements. In the more general case of a stage where critical flow conditions could be encountered at a larger number of locations (the blade end regions are generally the most suspect), a more complex situation exists.

The lower diffusion factor at stall with 0.22 tip radial distortion indicates that D alone was not always sufficient to signal critical flow conditions in the rotor tip region. The diffusion factor, of course, gave some measure of the blade suction surface velocity diffusion. Two additional flow conditions which very likely affected the critical nature of the flow in the tip region were the outer-casing, boundary-layer flow and the flow across the blade passage shock with its tendency for separation. Parameters used to give some measure of these two flow effects are a wall static-pressure-rise coefficient, defined as

$$\left(\frac{p_2 - p_1}{P_1 - p_1}\right)_{wall} \tag{4}$$

and a shock static-pressure-rise coefficient, defined as

$$\left(\frac{p_{shock,out} - p_{shock,in}}{P'_{shock,in} - p_{shock,in}}\right)_{shock} \tag{5}$$

All the values in expression (5) can be obtained from compressible flow tables. The blade surface Mach number into the shock was approximated from the blade inlet relative Mach number and a supersonic expansion equal to the incidence angle to the blade suction surface. When the blade inlet relative Mach number was less than 1.0, the expansion was taken from a Mach number of 1.0; and the calculated surface Mach number was

reduced by the ratio of the blade inlet relative Mach number to a Mach number of 1.0. The accuracy of this latter procedure is not known, but it is a consistent method for calculating surface Mach numbers at inlet Mach numbers slightly less than 1.0. The parameters of expressions (4) and (5), as well as some selected blade-element parameters measured at the blade element located 7 percent of the span height from the tip, are summarized in table IV. Values at near-stall operation for all configurations and all speeds tested are shown.

Examination of the data of table IV indicates that no single parameter provided a consistent indicator of stall (or near stall) flow conditions for all operating speeds. Also, a general relation indicating the influence of the individual parameters on critical (imminent stall) flow conditions was not apparent. General trends of stalling diffusion factor with the wall pressure-rise coefficient and axial velocity ratio are indicated by the plots in figures 11 and 12. The trends of a decreasing stalling diffusion factor with increasing magnitudes of wall pressure-rise coefficient and axial velocity ratio are generally apparent despite some scatter of the data. Additional analysis is needed to determine the general applicability of these data, as well as to establish the effect of these parameters on critical flow conditions.

The condition of the wall boundary layer entering the blade row is also a parameter of interest. Unfortunately, the wall boundary layer was not sufficiently defined in this set of data for use as a correlating parameter, even though the presence of the tip and hub distortion screens may be affecting the size of inlet wall boundary layers.

Additional factors affecting the results may be the data accuracy, particularly with respect to measuring static pressures close to a wall, and the need to define more accurately the true streamlines at these off-design flow conditions. In all operating conditions, the streamlines were assumed to be the same, that is, those defined in the design calculations.

Operation at Choke-Flow Conditions

The overall performance characteristic curves (with and without distortion) at design speed indicate (1) that choking was occurring within the rotor blade row (as evidenced by the vertical portion of the overall characteristic at the highest flow rate); and (2) that as the inlet flow was distorted, the choking weight flow decreased from that with undistorted inlet flow. In figure 13 the radial distributions of selected blade-element parameters at choking weight flows (as represented by data at lowest pressure ratios in fig. 7) are shown for all cases. Emphasis is on comparisons and similarities in the parameters rather than on the absolute level of any particular set of test conditions.

The radial distribution plots primarily point out the difficulty of estimating choke-flow conditions (which occur within the blade passage) from flow conditions measured at

the blade inlet and outlet stations. In particular the radial distributions of axial velocity at the blade inlet (fig. 13(c)) and outlet (fig. 13(n)) indicate that mass flow shifts (hence streamline or streamtube location) across the blade row were significantly different with and without inlet flow distortion. With present analytical procedures the local flow areas of the individual streamtubes cannot be calculated for an off-design operating condition. The definition of streamlines for each operating condition are needed both to provide geometric flow area through the passage and to allow calculation of the total relative conditions (P' and T', which set the critical flow area A^*) along the flow path.

It is of interest that an absolute flow Mach number of 1.0 at the blade leading edge (fig. 13(d)) was calculated at a near midspan location for the most severe tip radial distortion. Radial distributions of corrected specific flow (fig. 13(e)) showed that in the midspan region values close to a maximum value of 241.1 kg/(sec)(m^2) (49.4 lbf/(sec)(ft^2)) were calculated for all operating conditions shown.

The five points whose detailed flow conditions are shown in figure 13 are represented as choke-flow operation. Actually, all the points on the vertical portions of the overall operating characteristics (fig. 6) represent choke-flow operation. For example, with a tip radial distortion of 22 percent the complete stable operating range shows a flow variation of about 0.45 kilogram per second (1 lbf/sec). Comparison of the radial distribution of inlet flow parameters (e.g., $V_{z,1}$ and i_{ss}) at choke (fig. 13) and near stall (fig. 10) shows very nearly the same levels and distributions. The outlet flow conditions for these two operating conditions were, of course, significantly different. Hence, the need to estimate flow conditions and areas within the blade row in order to establish choke-flow criteria is evident.

The data shown in figure 13(e) indicate that all radial distortions resulted in distributions of flow at the rotor inlet that were more peaked (in the midspan region) than the undistorted inlet flow. The peaked distributions resulted in a lower maximum flow that could be passed by the rotor. It is also of interest that the difference between the peak values of ρV_z for any radial distortion and ρV_z for undistorted flow relates directly to the deficit in maximum flow (with distortion) from the undistorted flow value.

Blade-Element Parameters at Design Speed

The analysis and prediction of compressor blade row performance is based largely on the operation of the individual blade elements and on summing this element performance in some manner to obtain the blade overall performance. The blade-element flow conditions are, of course, always related through continuity and equilibrium requirements. If we assume that flow with radial inlet distortion extending completely around the periphery is axisymmetric, the calculation of such flows could be carried out by using the same off-design calculation techniques used for undistorted inlet flow. This

requires some knowledge of blade-element performance at off-design operating conditions. In this section the variation of selected blade-element parameters over an operating range both with and without inlet distortion are presented to illustrate off-design operation. Data for a tip and hub blade element at design speed are shown in figure 14.

The parameters shown include incidence angle, loss coefficient, diffusion factor, axial velocity ratio, total pressure ratio, and fluid turning (shown by deviation angle). The hub-element loss coefficient values for the 0.15 hub radial distortion were negative and are not shown. These parameters tended to vary significantly with operating condition and primarily set the performance of the blade element. Again, the discussion emphasizes the changes (from undistorted inlet flow) as an inlet flow distortion was applied.

In general, the data shown in figure 14 reflect the flow processes discussed in the section Operation at the Same Flow. When inlet radial distortion was applied, the elements operated with significantly different magnitudes of incidence angle and axial velocity ratio. Both these parameters affected the blade loading (as indicated by diffusion factor) such that the overall range of diffusion factor was approximately the same. The significance of this as applied to an off-design calculation procedure is twofold:

(1) Both the inlet flow conditions and the flow changes across the blade row must be considered for calculation of off-design blade-element performance. This implies an iterative procedure. In terms of the parameters shown, the loss coefficient $\bar{\omega}$ and the deviation angle δ are affected by the axial velocity ratio $V_{z,2}/V_{z,1}$; but $\bar{\omega}$, in turn, affects the density rise and hence the $V_{z,2}/V_{z,1}$. Thus, the need for iteration to a converged solution.

(2) The flow model used to input the loss and the fluid turning (or deviation angle) must reflect the effects of the various combinations of incidence angle i and $V_{z,2}/V_{z,1}$ present for the same levels of overall blade loading.

Probably the most significant general effect shown by this set of data is that of axial velocity ratio. As the axial velocity ratio increased (for approximately the same blade loading), (1) losses and deviation angle tended to decrease (particularly the deviation angle) and (2) pressure ratio tended to increase. This trend is more evident from the tip-element data only. A quantitative analysis of this effect of these data was not attempted. The trend was noted and the need to recognize this effect in correlation or analysis of data is suggested. These observations in items 1 and 2 also illustrate that for a given level of blade loading (diffusion factor), the energy addition (pressure ratio) increased and the deviation angle and loss coefficient decreased as axial velocity across the blade row was increased.

It is recognized that the elements shown are those reasonably close to the annulus walls and that the effects indicated could reflect the effects of axial velocity ratio on the annulus wall boundary layer flows. However, similar trends with axial velocity ratio at other elements along the span can be noted from radial variations of the parameters shown in figures 8, 10, and 13.

CONCLUSIONS

A single rotating blade row was tested with two magnitudes of tip radial distortion and two magnitudes of hub radial distortion imposed on the inlet flow. Comparisons of performance and flow parameters based on measured performance with undistorted inlet flow allow some observations of the effects of inlet flow distortion on rotor operation. The rotor was approximately 50 centimeters (20 in.) in diameter and had a design operating tip speed of approximately 420 meters per second (1380 ft/sec). Data obtained at 60, 80, and 100 percent of design speed are presented. Both overall performance and selected blade-element performance parameters are shown. Emphasis throughout is placed on the changes in flow and in rotor performance produced by radial inlet flow distortion as compared with those produced by undistorted inlet flow conditions.

The overall performance comparisons indicated the following results:

1. With tip radial distortion, there was a general decrease in the stall line pressure ratio and a decrease in the rotor stall margin.

2. With hub radial distortion, there was generally no change or some increase in the stall line pressure ratio and rotor stall margin.

3. With either type of distortion, and regardless of magnitude, there was a decrease in choke-flow rate at design speed. At the lower speeds there were smaller decreases or no change in the choke-flow rate.

Comparisons of radial distributions of blade-element parameters at design speed indicated the following:

1. At the same flow rate, the blade elements operated at higher incidence angles in the distorted flow regions (either hub or tip), where the inlet total pressure was reduced, and at lower incidence angles in the undistorted flow regions, where inlet total pressure was high. The result of this combination of inlet flow conditions was that the magnitude of total pressure at the rotor outlet was reduced at all radii (from that produced with undistorted inlet flow).

2. At near-stall operation, the highest levels of blade loading, as evidenced by diffusion factor or total temperature rise, occurred in the tip region. This indicates that rotor stall was initiated when certain critical flow conditions in the blade tip regions were attained. At design speed, near-stall operation for all cases showed a diffusion factor at the blade element located 7 percent of span from the rotor tip of about 0.63 for all operation except with the highest level of tip radial distortion, at which the near-stall diffusion factor was 0.50. This latter diffusion factor was accompanied by relatively high values of wall static-pressure-rise coefficient and axial velocity ratio. Correlation of near-stall operation at all speeds showed a general trend of lower diffusion factors with increasing wall static-pressure-rise coefficient and axial velocity ratio.

3. At choke-flow operation, the radial distributions of axial velocity, Mach number, and specific flow at the blade inlet showed higher local values with distortion than without

distortion; the higher the local value, the greater the decrease in maximum flow. However, a criterion for predicting maximum flow from inlet or outlet flow distributions was not apparent.

The operation of hub and tip blade elements with hub radial and tip radial distortion was presented for design-speed operation. These performance data illustrated the type of input data and calculation techniques required to calculate performance with radial distortion as an off-design problem.

Lewis Research Center,
National Aeronautics and Space Administration,
Cleveland, Ohio, August 14, 1974,
501-24.

APPENDIX A

SYMBOLS

A area, m^2; ft^2

D diffusion factor, $1 - \frac{V'_{TE}}{V'_{LE}} + \frac{\left(rV_\theta\right)_{TE} - \left(rV_\theta\right)_{LE}}{(r_{LE} + r_{TE})\sigma V'_{LE}}$

i_{ss} incidence angle, angle between inlet air direction and line tangent to blade suction surface at leading edge, $\left(\beta'_m\right)_{LE} - \left(\kappa_{ss}\right)_{LE}$, deg

M Mach number

N rotor speed, rpm

P total pressure, N/cm^2; psia

PR pressure ratio

p static pressure, N/cm^2; psia

R gas constant, J/(kg)(K)

r radius, cm; in.

T total temperature, K; ^oR

ΔT temperature differential, K; ^oR

V air velocity, m/sec; ft/sec

W weight flow, kg/sec; lbm/sec

β air angle, angle between air velocity and axial direction, deg

γ ratio of specific heats, 1.40

δ ratio of inlet total pressure to standard pressure of 10.13 N/cm^2 (14.69 psia)

δ^o deviation angle, angle between exit air direction and tangent to blade mean-camber line at trailing edge, $\left(\beta'_m\right)_{TE} - \left(\kappa_{mc}\right)_{LE}$, deg

η temperature-rise efficiency

θ ratio of inlet total temperature to standard temperature of 288.2 K (518.7^o R)

κ_{mc} angle between blade mean-camber line at leading or trailing edge and axial direction, deg

κ_{ss} angle between blade suction-surface camber line at leading edge and axial direction, deg

ρ density

σ solidity, ratio of chord to spacing, kg/m^3

$\bar{\omega}$ total-pressure-loss coefficient, $\dfrac{\left(P'_{id}\right)_{TE} - P'_{TE}}{P'_{LE} - p_{LE}}$

Subscripts:

ad adiabatic

av average

des design conditions

id ideal

ind indicated

LE blade leading edge

m meridional direction

max maximum

min minimum

s at stall

sur surface

TE blade trailing edge

z axial direction

θ tangential direction

1 upstream of rotor

2 downstream of rotor

Superscripts:

' relative to rotor

* critical

APPENDIX B

PERFORMANCE PARAMETERS

The performance parameters referred to in the main text are defined as follows:
Incidence angle based on suction-surface blade angle:

$$i_{ss} = \left(\beta'_m\right)_{LE} - \left(\kappa_{ss}\right)_{LE}$$

Deviation:

$$\delta^o = \left(\beta'_m\right)_{TE} - \left(\kappa_{mc}\right)_{TE}$$

Diffusion factor:

$$D = 1 - \frac{V'_{TE}}{V'_{LE}} + \frac{\left(rV_\theta\right)_{TE} - \left(rV_\theta\right)_{LE}}{(r_{LE} + r_{TE})\sigma V'_{LE}}$$

Total-pressure-loss coefficient:

$$\bar{\omega} = \frac{\left(P'_{id}\right)_{TE} - P'_{TE}}{P'_{LE} - p_{LE}}$$

Total loss parameter:

$$\frac{\bar{\omega} \cos\left(\beta'_m\right)_{TE}}{2\sigma}$$

Adiabatic efficiency:

$$\eta_{ad} = \frac{\left(\frac{P_{TE}}{P_{LE}}\right)^{(\gamma-1)/\gamma} - 1}{\frac{T_{TE}}{T_{LE}} - 1}$$

Equivalent weight flow:

$$\frac{W\sqrt{\theta}}{\delta}$$

Equivalent rotative speed:

$$\frac{N}{\sqrt{\theta}}$$

REFERENCES

1. Ball, Calvin L.; Janetzke, David C.; and Reid, Lonnie: Performance of 1380-Foot-Per-Second-Tip-Speed Axial-Flow Compressor Rotor With Blade Tip Solidity of 1.5. NASA TM X-2379, 1972.

2. Glawe, George E.; Krause, Lloyd N.; and Dudzinski, Thomas J.: A Small Combination Sensing Probe for Measurement of Temperature, Pressure, and Flow Direction. NASA TN D-4816, 1968.

TABLE I. - DESIGN OVERALL PARAMETERS FOR ROTOR 5

Total pressure ratio	1.652
Total temperature ratio	1.187
Efficiency	0.824
Weight flow per unit frontal area, kg/(sec)(m^2)	1.291
Weight flow per unit annulus area, kg/(sec)(m^2)	1.732
Weight flow, kg/sec	29.612
Rotor speed, rpm	16 000
Tip speed, m/sec	420.687

TABLE II. - DISTORTION PARAMETER VALUES OVER OPERATING RANGE

Rotor speed, N, percent of design	Corrected weight flow, $W\sqrt{\theta}/\delta$, kg/sec	Ratio of equivalent weight flow to design, $\frac{W\sqrt{\theta}/\delta}{(W\sqrt{\theta}/\delta)_{des}}$	Maximum total pressure, P_{max}, N/cm^2	Minimum total pressure, P_{min}, N/cm^2	Distortion indices	
					$\frac{P_{max} - P_{min}}{P_{max}}$	$\frac{P_{av} - P_{min}}{P_{av}}$
Tip radial distortion, 0.15						
100	29.32	0.990	10.74	9.07	0.155	0.104
	28.96	.978	10.73	9.11	.150	.100
80	26.24	.886	10.59	9.34	.118	.078
	24.04	.812	10.50	9.50	.095	.062
60	21.71	.733	10.42	9.63	.075	.049
	17.54	.592	10.31	9.82	.047	.031
Tip radial distortion, 0.22						
100	28.83	0.973	10.92	8.40	0.230	0.170
	28.35	.957	10.89	8.51	.219	.160
90	27.00	.912	10.78	8.68	.195	.143
80	26.02	.879	10.71	8.83	.176	.128
	24.79	.837	10.66	8.96	.159	.115
60	22.68	.766	10.54	9.21	.126	.091
	18.22	.615	10.38	9.56	.080	.057
Hub radial distortion, 0.05						
100	29.49	0.996	10.34	9.80	0.053	0.033
	27.81	.939	10.38	9.85	.051	.028
80	26.34	.890	10.30	9.90	.039	.022
	24.19	.817	10.27	9.94	.032	.018
	20.76	.701	10.22	9.99	.023	.014
60	20.68	.698	10.23	9.99	.024	.014
	15.03	.507	10.18	10.07	.012	.006
Hub radial distortion, 0.11						
100	28.94	0.977	10.47	9.16	0.125	0.095
	26.09	.881	10.35	9.42	.090	.070
80	24.94	.842	10.37	9.49	.085	.063
	19.95	.674	10.25	9.75	.048	.037
60	18.80	.635	10.25	9.82	.042	.031
	14.63	.494	10.19	9.94	.025	.019

TABLE III. - SUMMARY OF EFFECT OF INLET FLOW DISTORTION ON STALL PRESSURE RATIO

Rotor speed, N, percent of design	Stall pressure ratio, $(PR)_{s,distorted}$	$\left[\frac{(PR)_{s,distorted} - (PR)_{s,undistorted}}{(PR)_{s,undistorted}}\right]_{N/\sqrt{\theta}=Constant} \times 100$, percent	$\left[\frac{(PR)_{s,distorted} - (PR)_{s,undistorted}}{(PR)_{s,undistorted}}\right]_{W\sqrt{\theta}/\delta=Constant} \times 100$, percent
No distortion			
100	1.800	------	-----
80	1.460	------	-----
60	1.245	------	-----
Tip radial distortion, 0.15			
100	1.785	-0.83	-5.1
80	1.455	-.34	-7.9
60	1.230	-1.21	-7.5
Tip radial distortion, 0.22			
100	1.610	-10.56	-11.5
80	1.400	-4.11	-13.6
60	1.210	-2.81	-11.0
Hub radial distortion, 0.05			
100	1.805	0.28	1.1
80	1.460	0	1.0
60	1.240	-.40	.4
Hub radial distortion, 0.11			
100	1.830	1.67	8.9
80	1.470	.69	4.3
60	1.240	-.40	.8

TABLE IV. - SUMMARY OF BLADE-ELEMENT PARAMETERS FOR 7-PERCENT-OF-SPAN ELEMENT AT NEAR-STALL OPERATION

Rotor speed, N, percent of design	Inlet Mach number relative to rotor, M_1'	Incidence angle, i_{ss}, deg	Surface Mach number relative to rotor, M_{sur}'	Shock static-pressure-rise coefficient, $\left(\frac{p_{shock,out} - p_{shock,in}}{p'_{shock,in} - p_{shock,in}}\right)_{shock}$	Diffusion factor, D	Temperature rise corrected to design speed, $\Delta T\left(\frac{N_{des}}{N}\right)^2$, K	Wall static-pressure-rise coefficient, $\left(\frac{p_2 - p_1}{p_1 - p_1}\right)_{wall}$	Axial velocity ratio, $V_{z,2}/V_{z,1}$
Undistorted flow								
60	0.760	7.5	1.025	-----	0.596	80.9	4.24	0.912
100	1.358	2.9	1.458	0.535	.628	82.8	3.26	.782
Tip radial distortion, 0.15								
60	0.733	9.7	1.045	-----	0.570	77.9	5.21	1.089
70	.871	8.2	1.197	0.357	.535	77.6	5.02	1.092
80	.998	7.4	1.343	.484	.568	77.3	4.91	1.020
90	1.136	5.8	1.361	.494	.569	80.0	4.55	.991
100	1.270	5.4	1.461	.536	.616	85.1	4.52	.921
Tip radial distortion, 0.22								
60	0.718	10.8	1.050	-----	0.567	80.2	6.03	1.250
70	.852	9.9	1.220	0.383	.551	77.9	5.60	1.222
80	.980	8.8	1.367	.497	.480	74.2	5.67	1.298
90	1.114	8.0	1.422	.522	.530	73.4	5.28	1.180
100	1.241	7.9	1.520	.550	.504	73.4	5.22	1.222
Hub radial distortion, 0.05								
60	0.752	8.3	1.035	-----	0.578	77.8	4.55	0.985
70	.891	7.2	1.192	0.351	.548	76.8	4.39	1.001
80	.922	7.5	1.244	.407	.534	74.5	3.54	1.112
90	1.153	5.0	1.346	.485	.586	77.8	4.08	.908
100	1.327	3.3	1.442	.530	.640	82.5	3.60	.769
Hub radial distortion, 0.11								
60	0.752	7.9	1.024	-----	0.612	82.4	4.31	0.913
70	.891	6.6	1.173	0.327	.534	76.8	4.07	1.005
80	1.025	6.0	1.300	.455	.555	78.1	4.05	.982
90	-----	---	-----	-----	-----	----	----	-----
100	1.326	3.2	1.438	.528	.634	83.7	3.41	.810

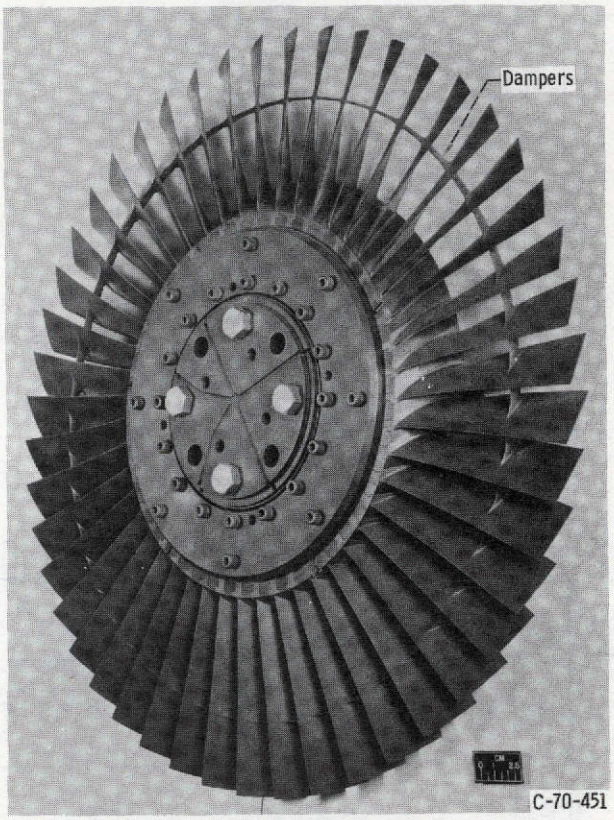

Figure 1. - Test rotor 5.

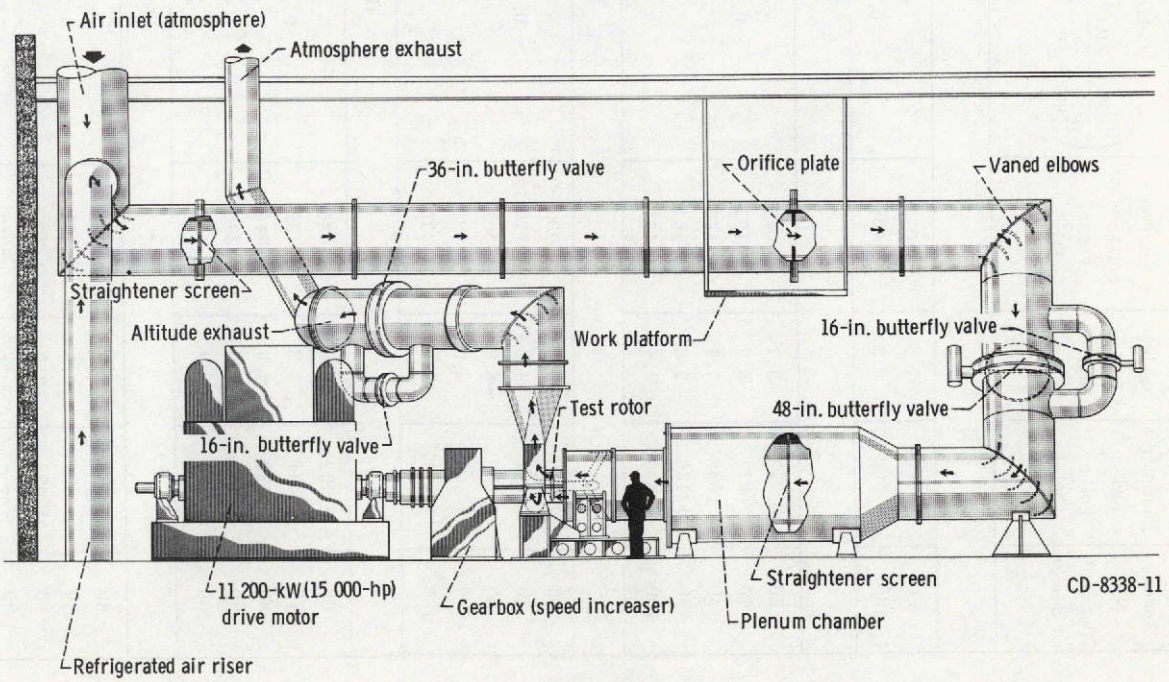

Figure 2. - Compressor test facility.

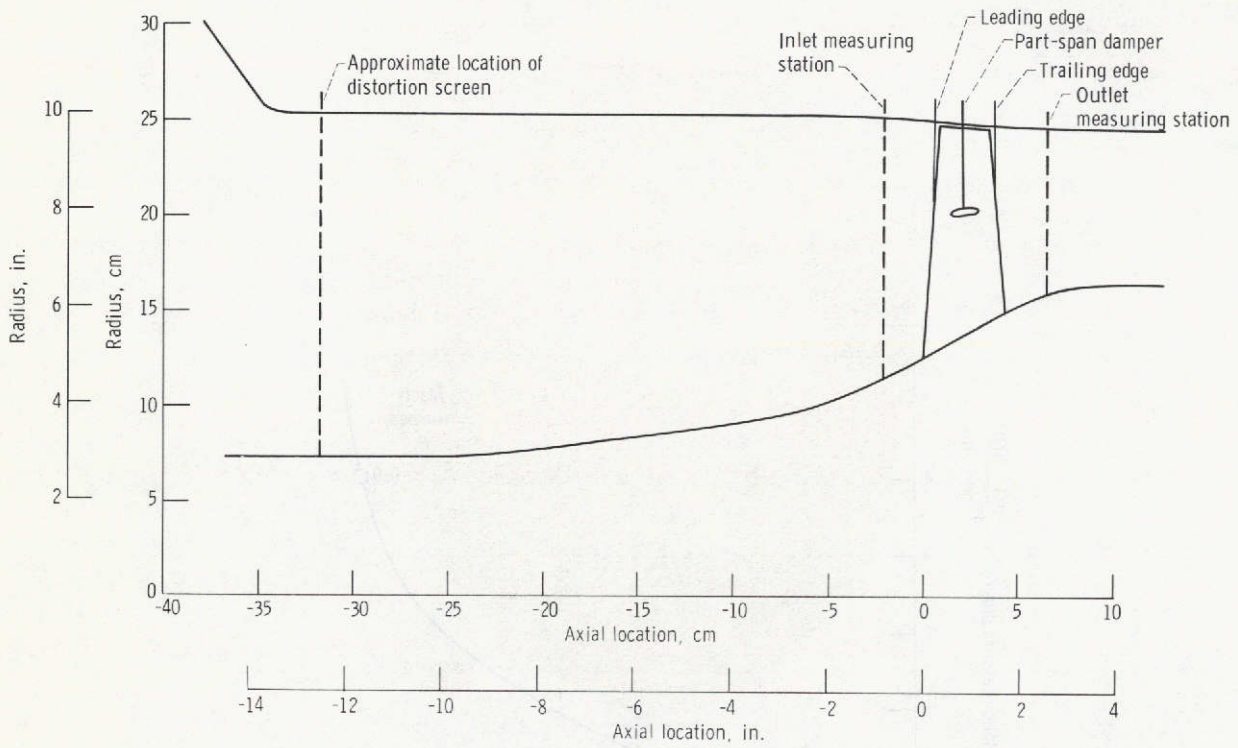

Figure 3. - Compressor flow path for rotor 5 distortion tests.

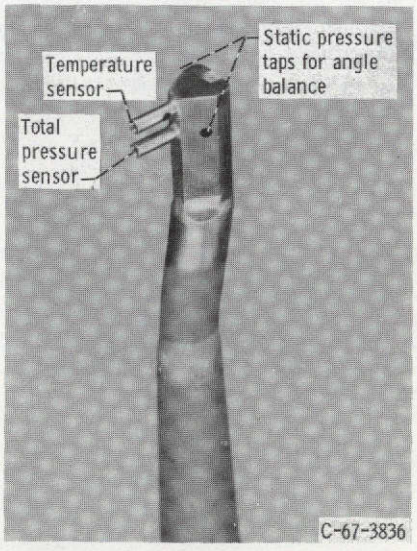

Figure 4. - Combination total pressure, total temperature, and flow angle probe (double barrel).

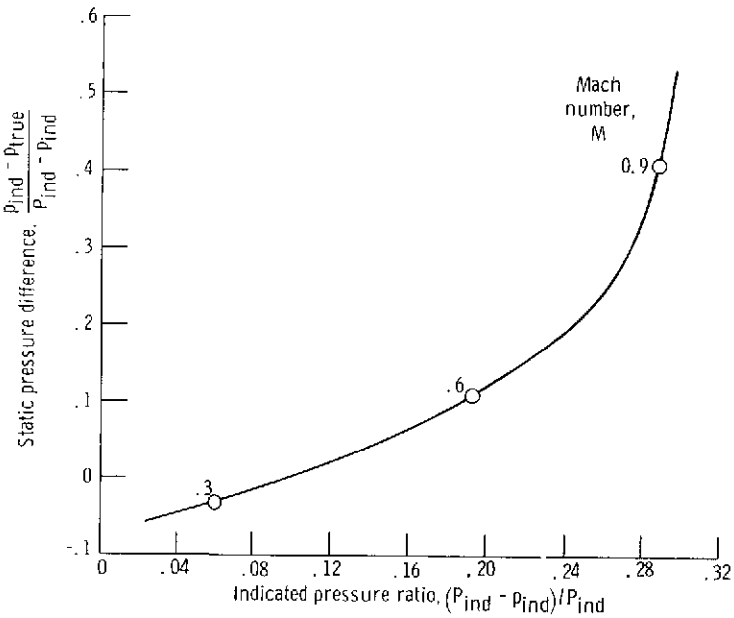

Figure 5. - Variation in static pressure difference with probe measurements for alined flow.

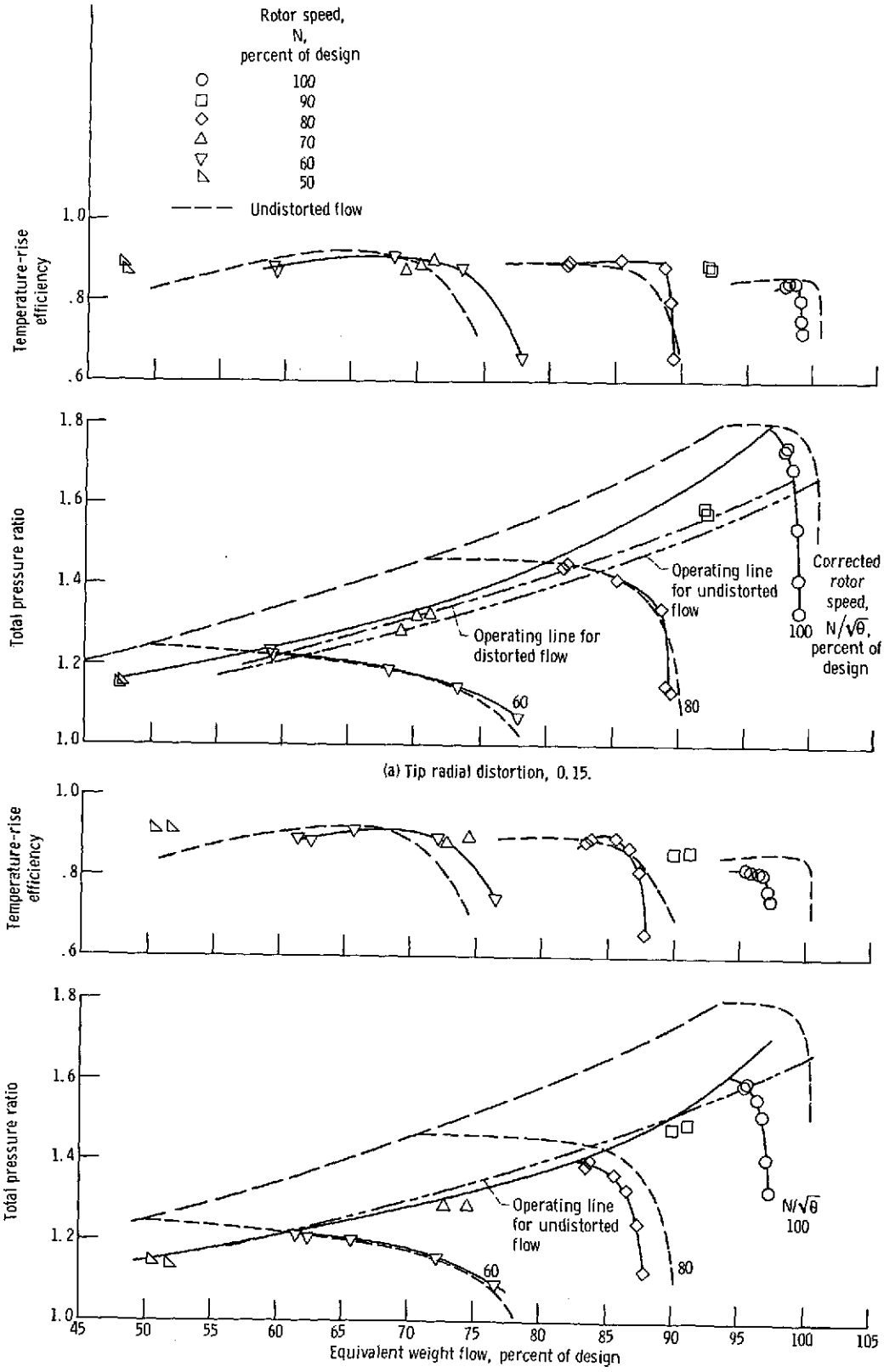

(a) Tip radial distortion, 0.15.

(b) Tip radial distortion, 0.22.

Figure 6. - Overall performance.

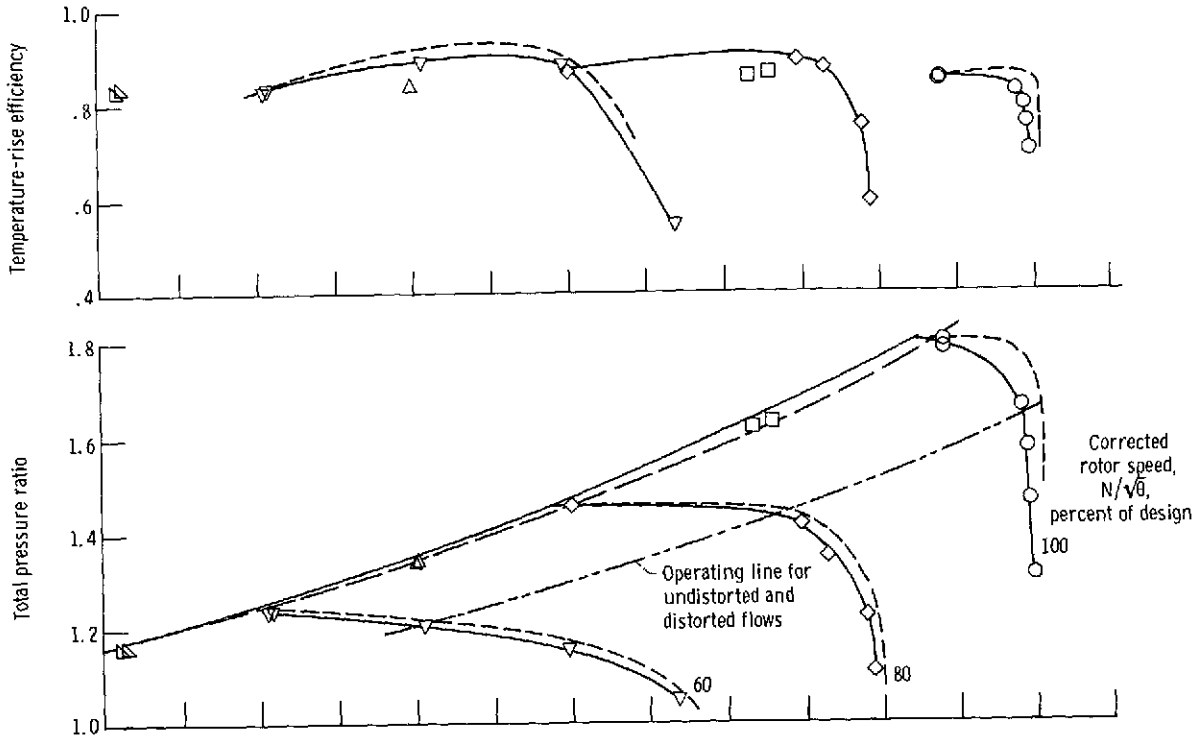

(c) Hub radial distortion, 0.05.

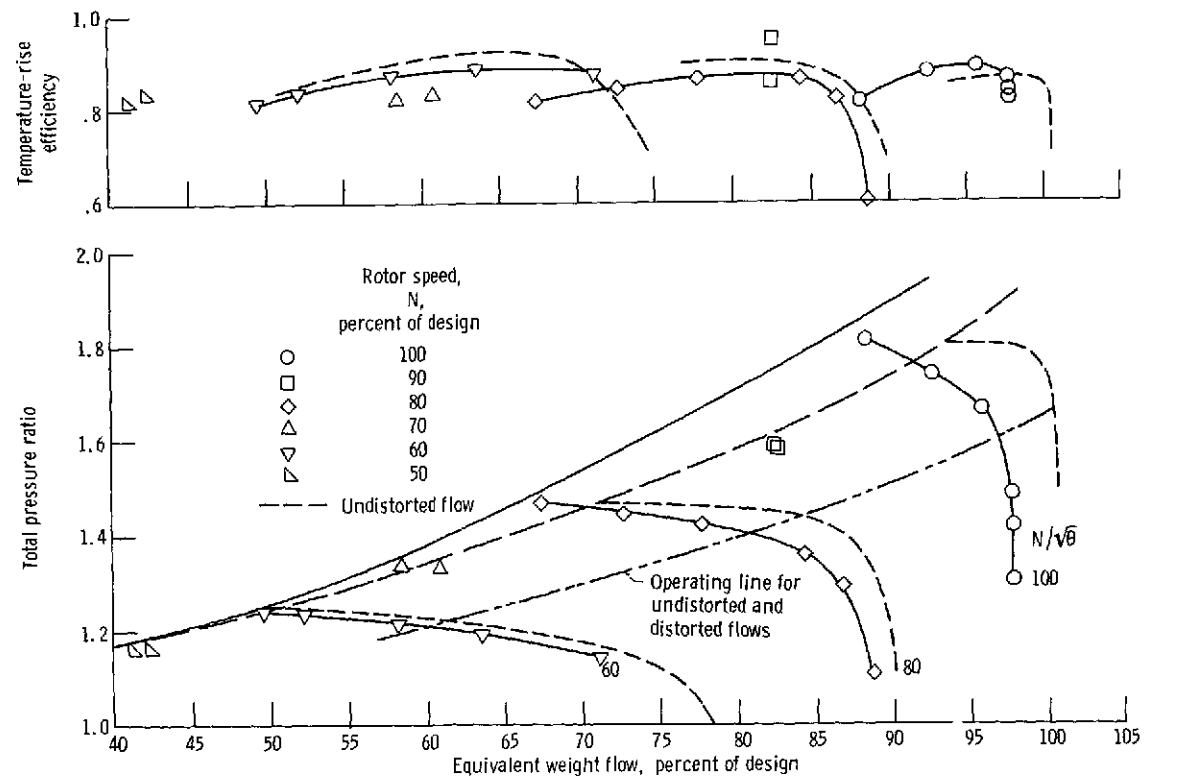

(d) Hub radial distortion, 0.11.

Figure 6. - Concluded.

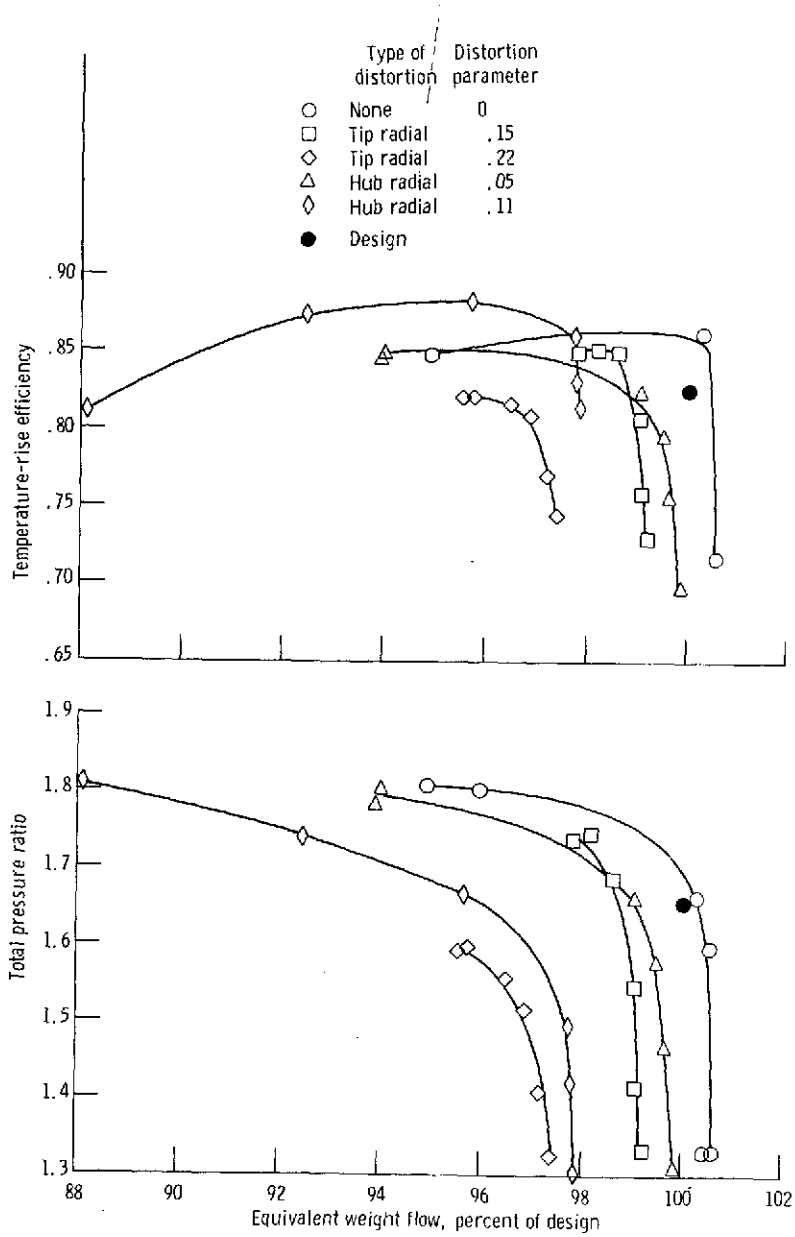

Figure 7. - Comparison of overall performance with and without distortion (design speed).

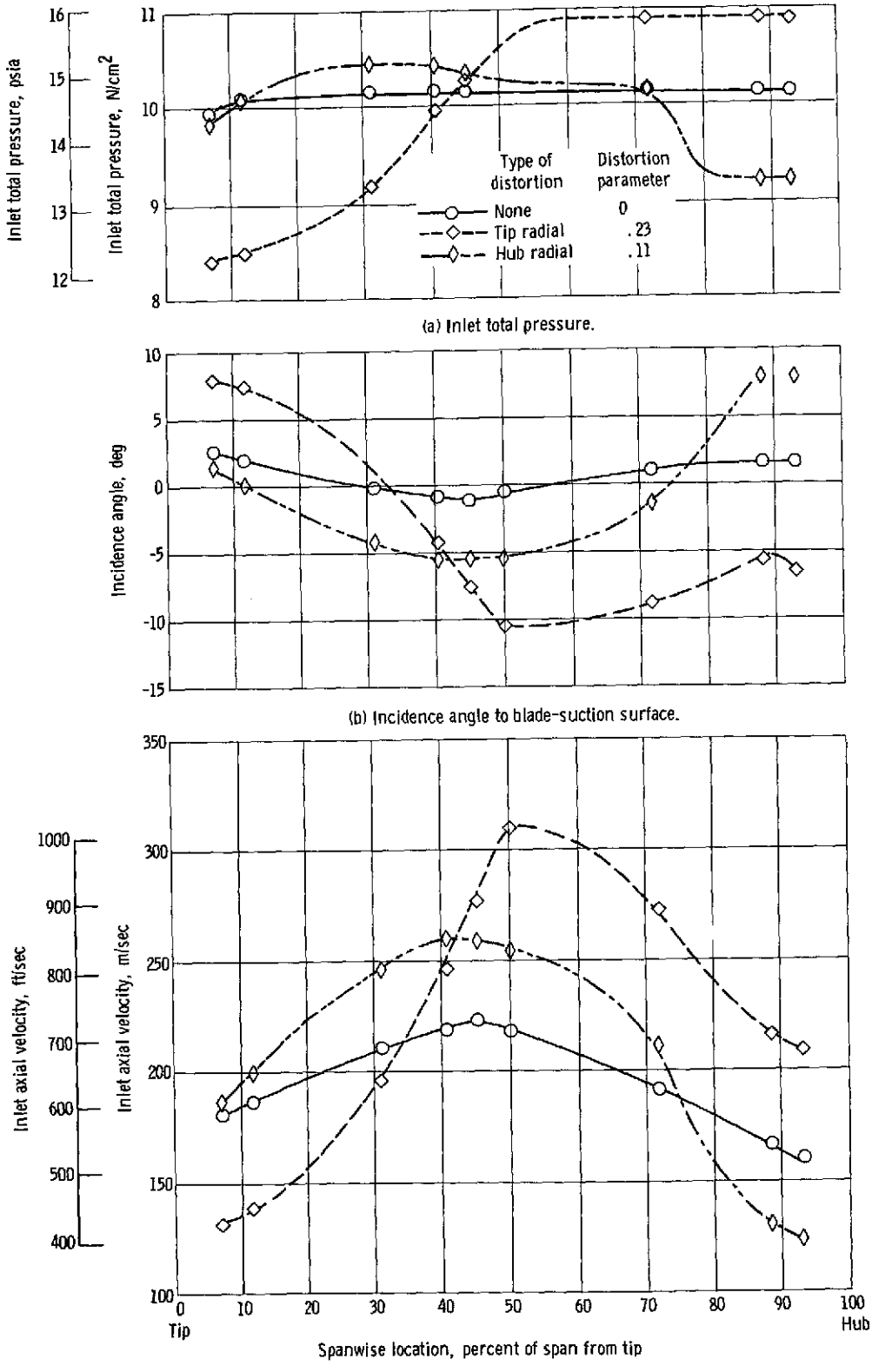

Figure 8. - Radial distributions of blade-element parameters at same flow with and without distortion (design speed). Corrected weight flow, $(W\sqrt{\theta}/\delta)/(W\sqrt{\theta}/\delta)_{des}$, 0.96.

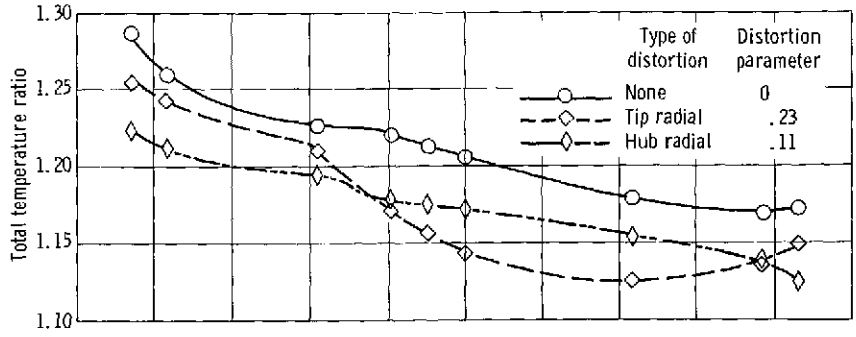

(d) Total temperature ratio.

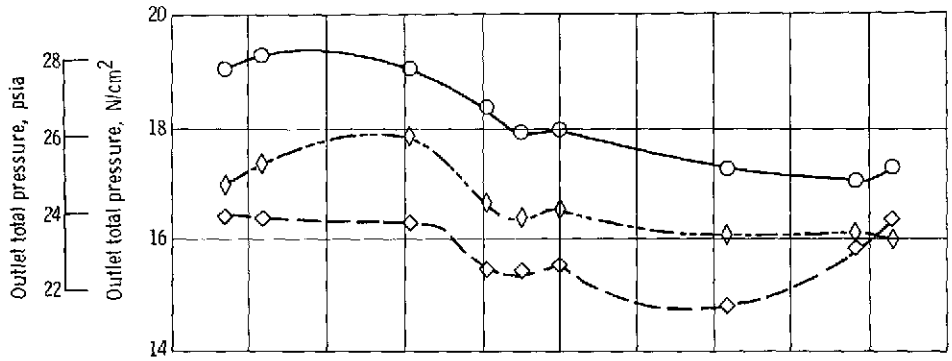

(e) Outlet total pressure.

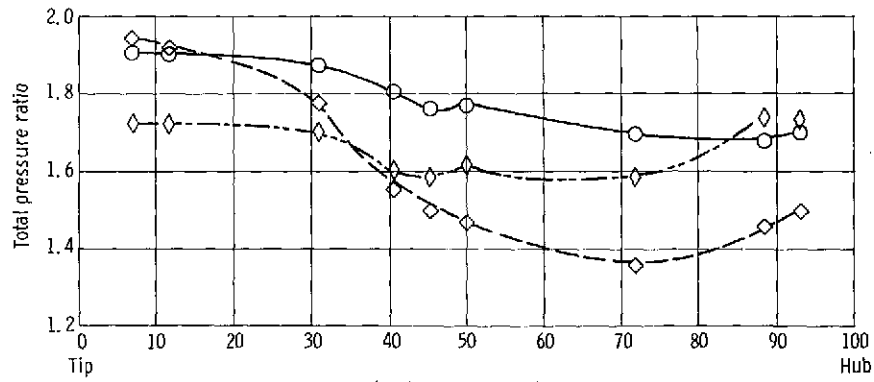

(f) Total pressure ratio.

Figure 8. - Continued.

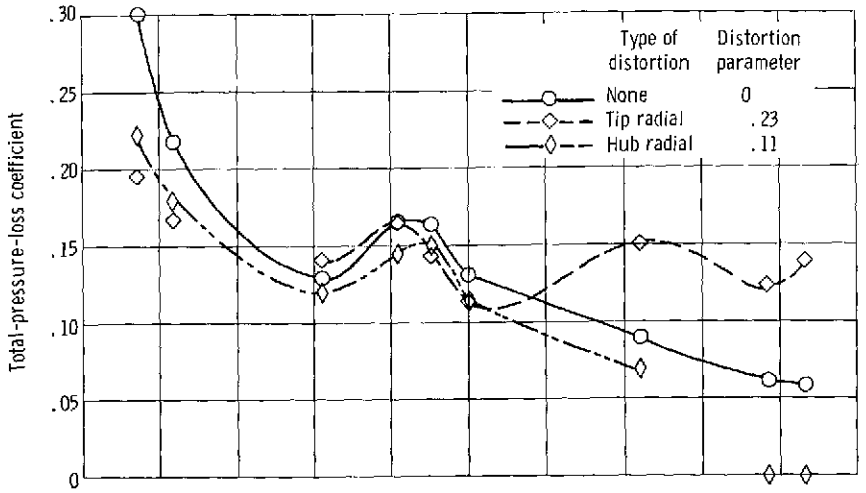

(g) Relative total-pressure-loss coefficient.

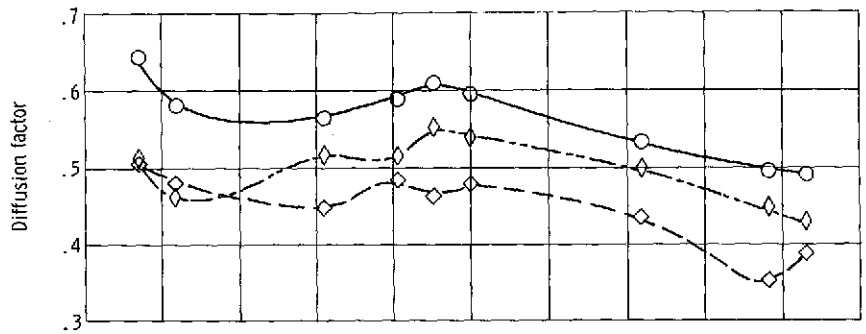

(h) Diffusion factor.

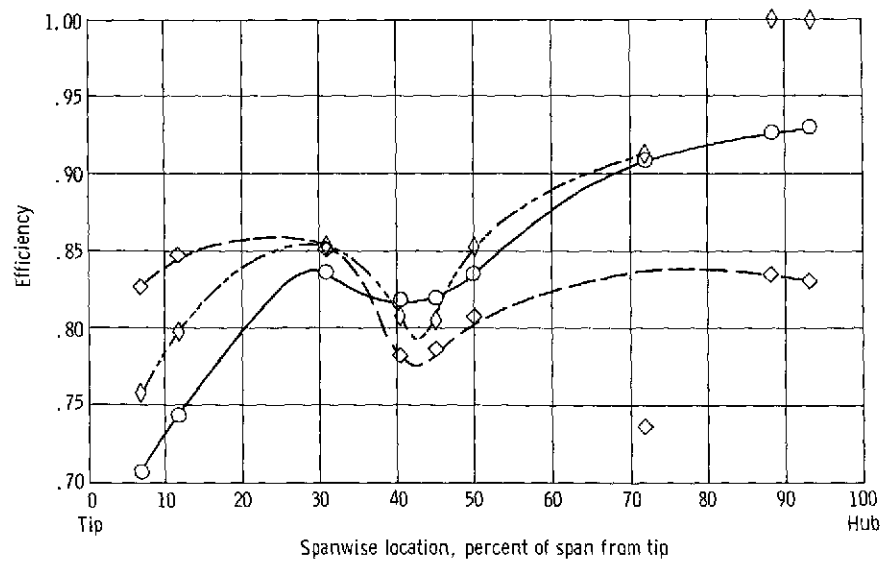

(i) Efficiency.

Figure 8. - Continued.

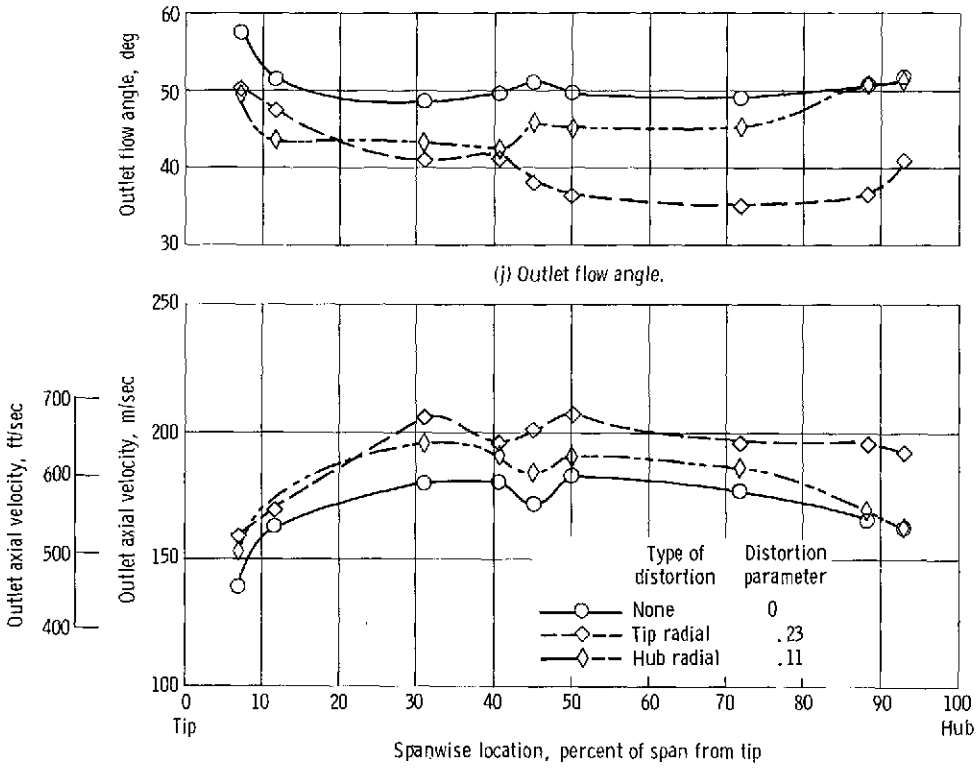

(j) Outlet flow angle.

(k) Outlet axial velocity.

Figure 8. - Concluded.

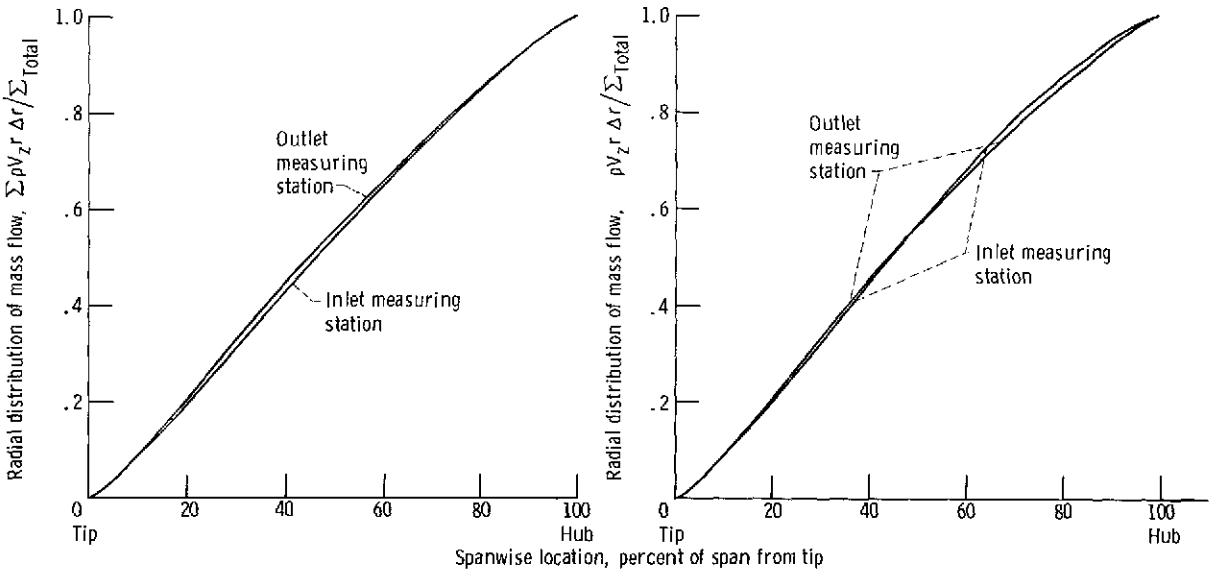

(a) Undistorted flow; weight flow, 28.45 kg/sec.

(b) Hub distortion, 0.11; weight flow, 28.30 kg/sec.

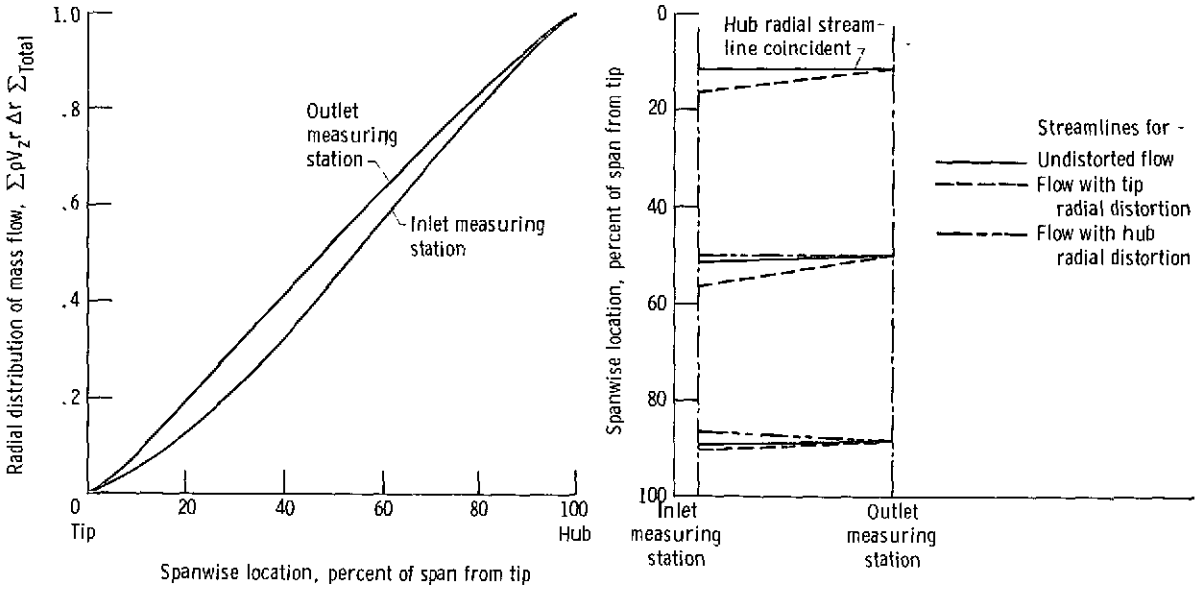

(c) Tip distortion, 0.22; weight flow, 28.35 kg/sec.

(d) Spanwise location of streamlines entering and leaving blade row.

Figure 9. - Radial variation of specific weight flow to indicate streamline shifts with and without distortion at same weight flow.

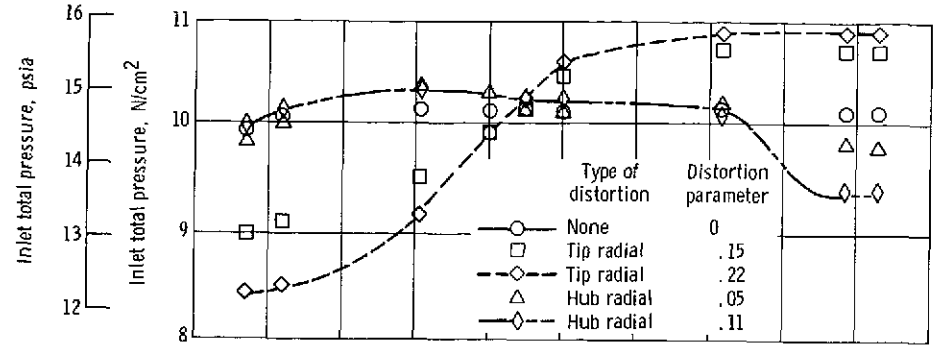

(a) Inlet total pressure.

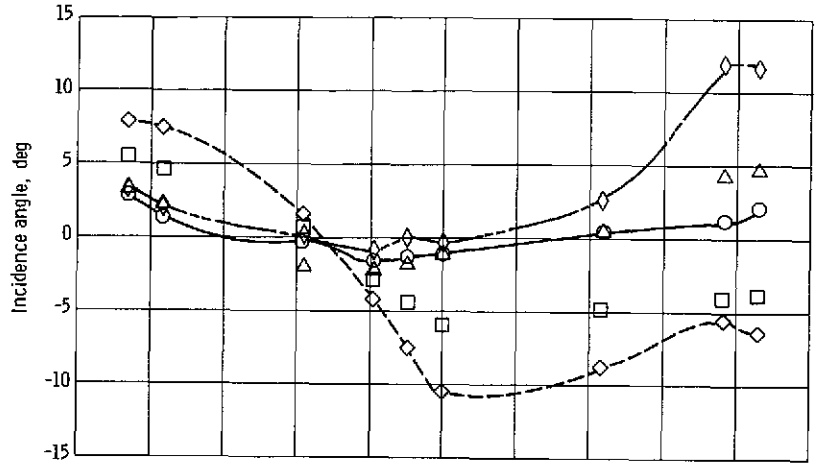

(b) Incidence angle to suction surface.

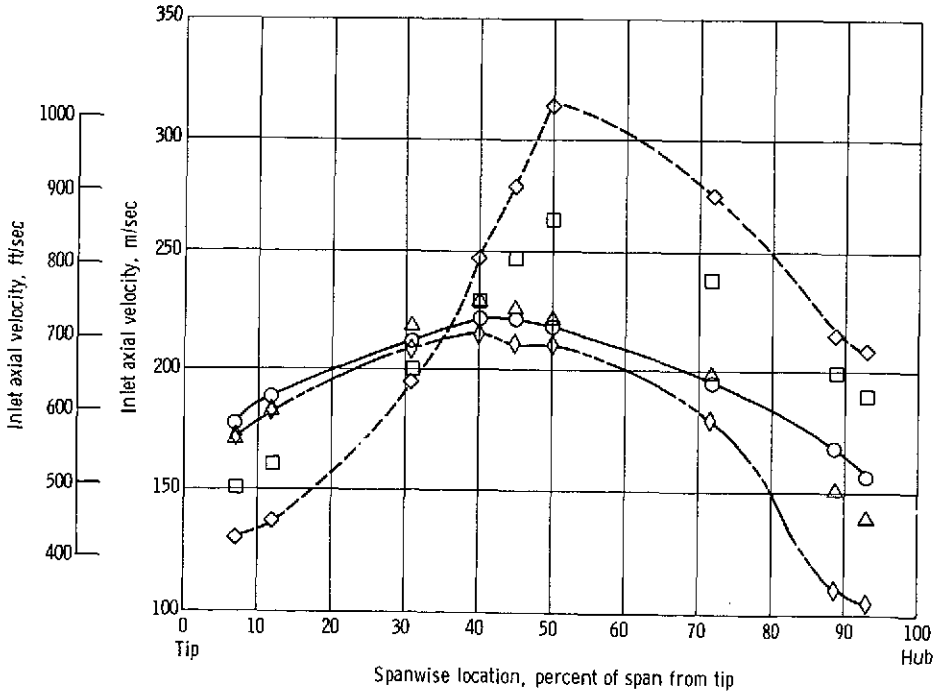

(c) Inlet axial velocity.

Figure 10. - Radial distributions of blade-element parameters at near-stall operation with and without distortion (design speed).

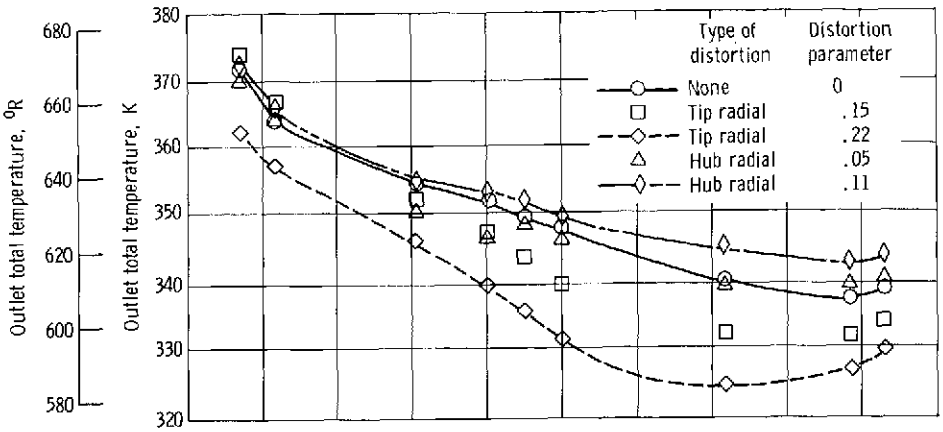

(d) Outlet total temperature.

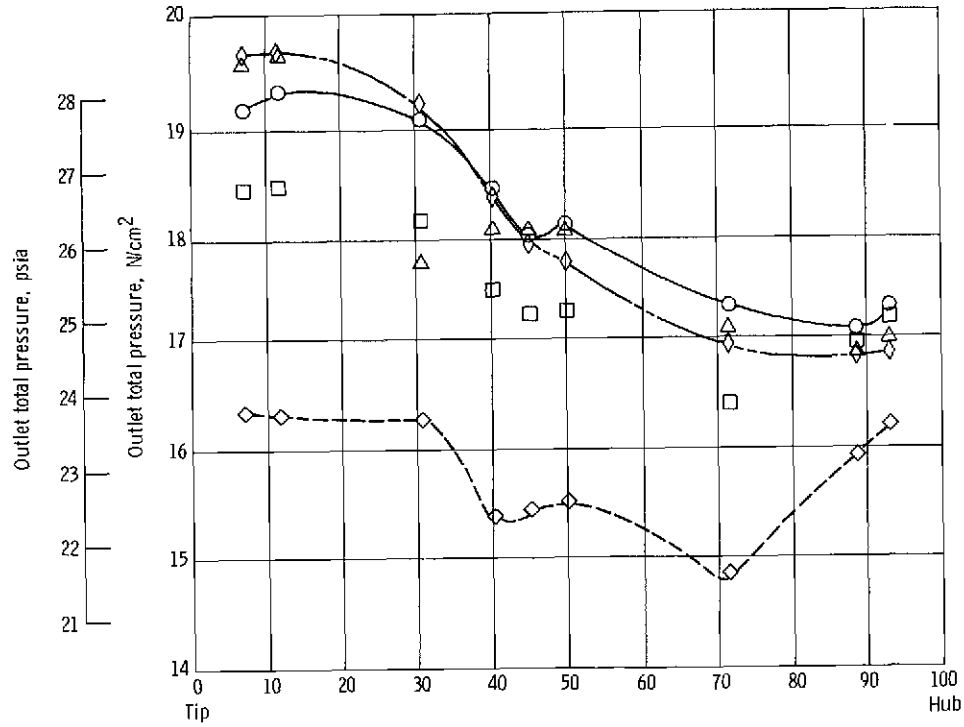

(e) Outlet total pressure.

Figure 10. - Continued.

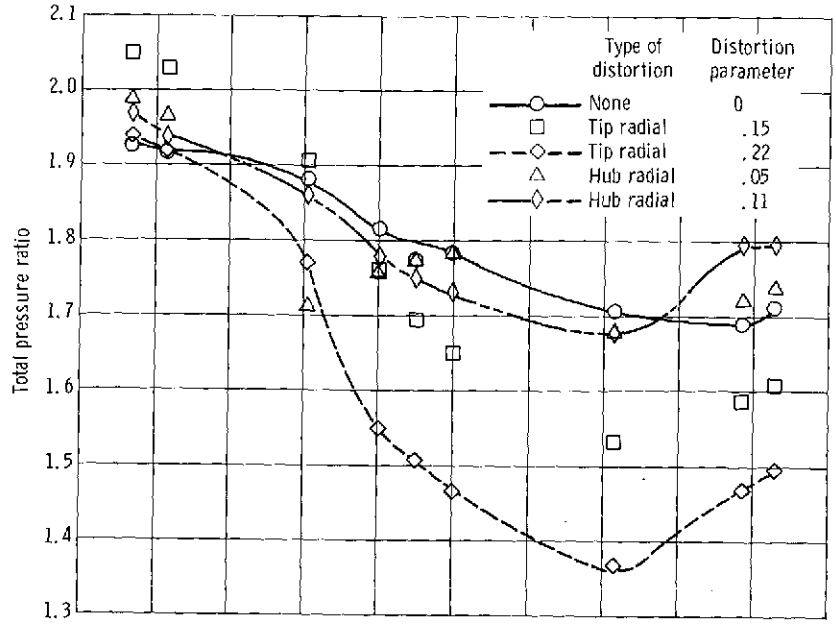

(f) Total pressure ratio.

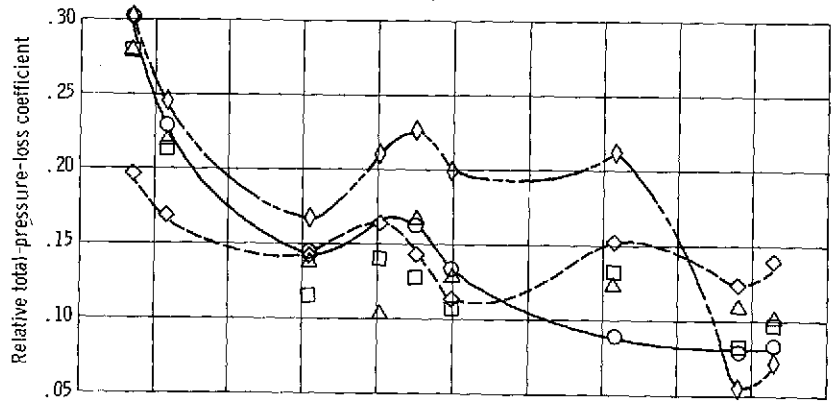

(g) Relative total-pressure-loss coefficient.

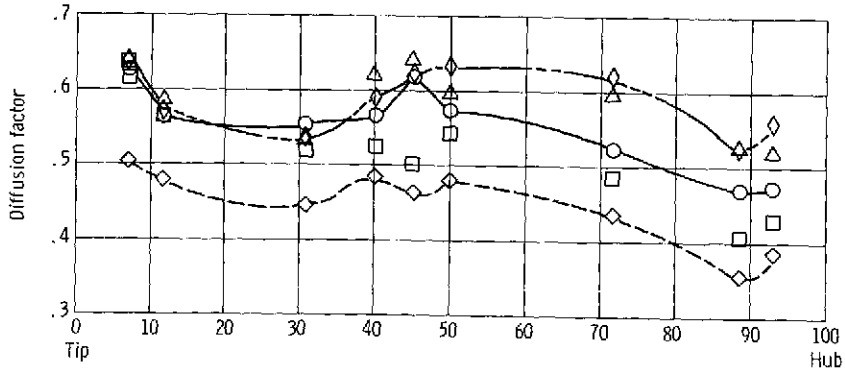

(h) Diffusion factor.

Figure 10. - Continued.

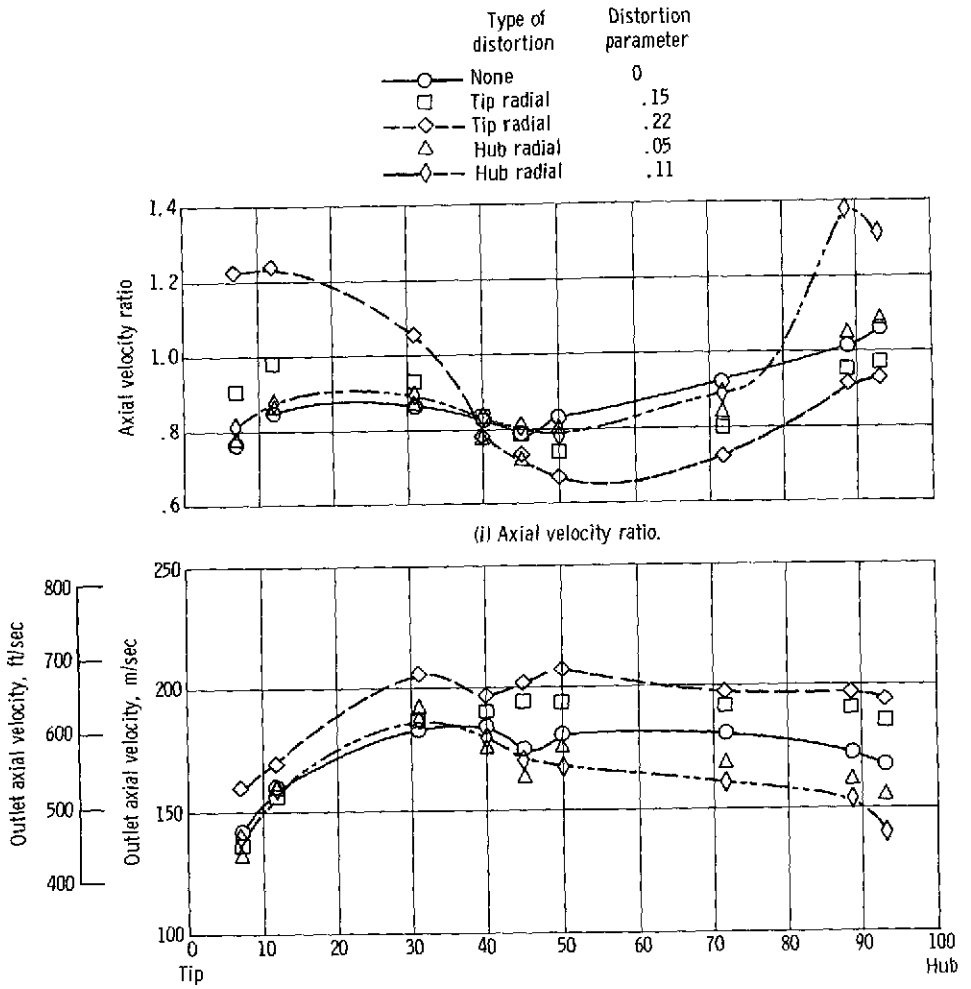

(i) Axial velocity ratio.

(j) Outlet axial velocity.

Figure 10. - Concluded.

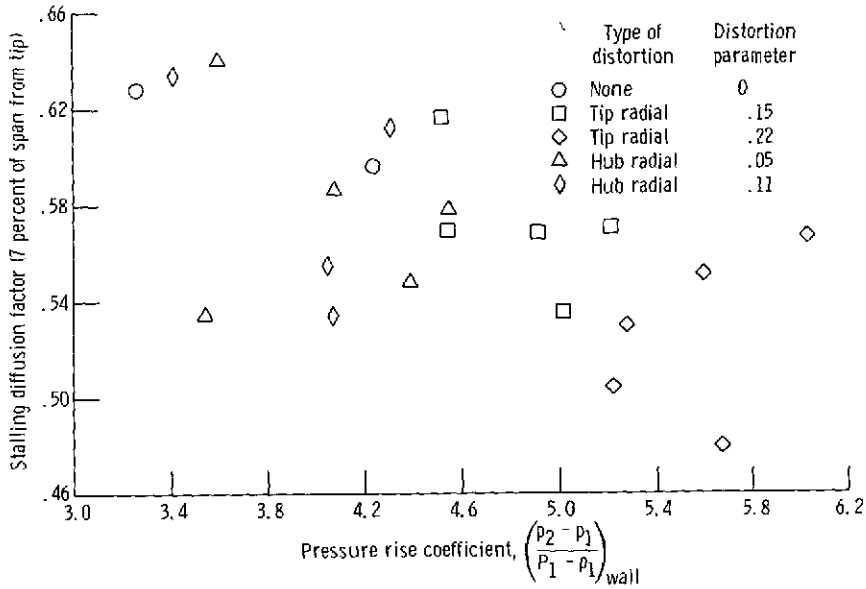

Figure 11. - Correlation of rotor tip diffusion factor with wall pressure-rise coefficient (near-stall operation).

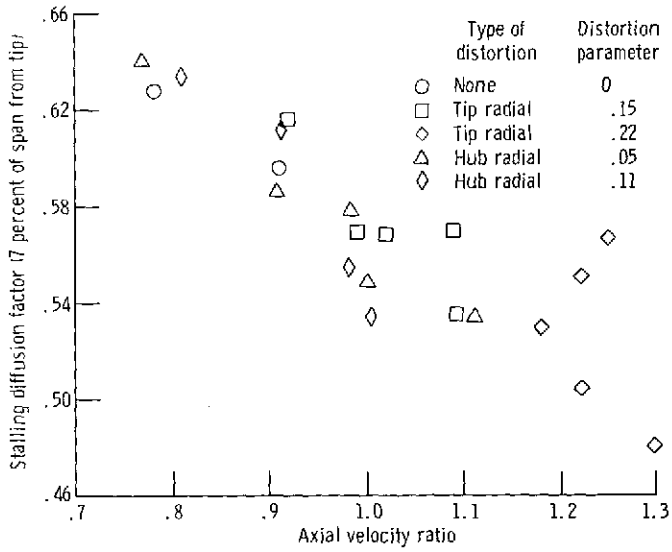

Figure 12. - Correlation of rotor tip diffusion factor with axial velocity ratio (near-stall operation).

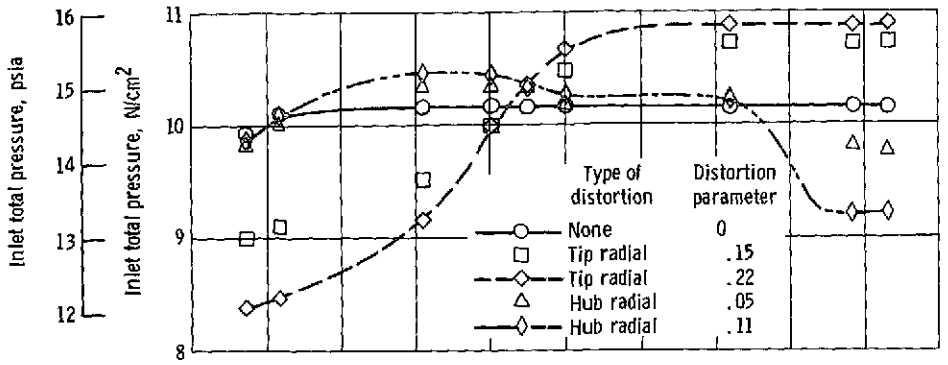

(a) Inlet total pressure.

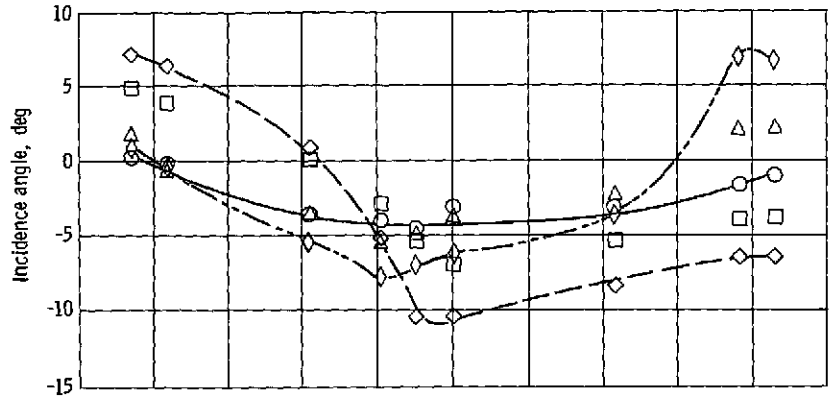

(b) Incidence angle to suction surface.

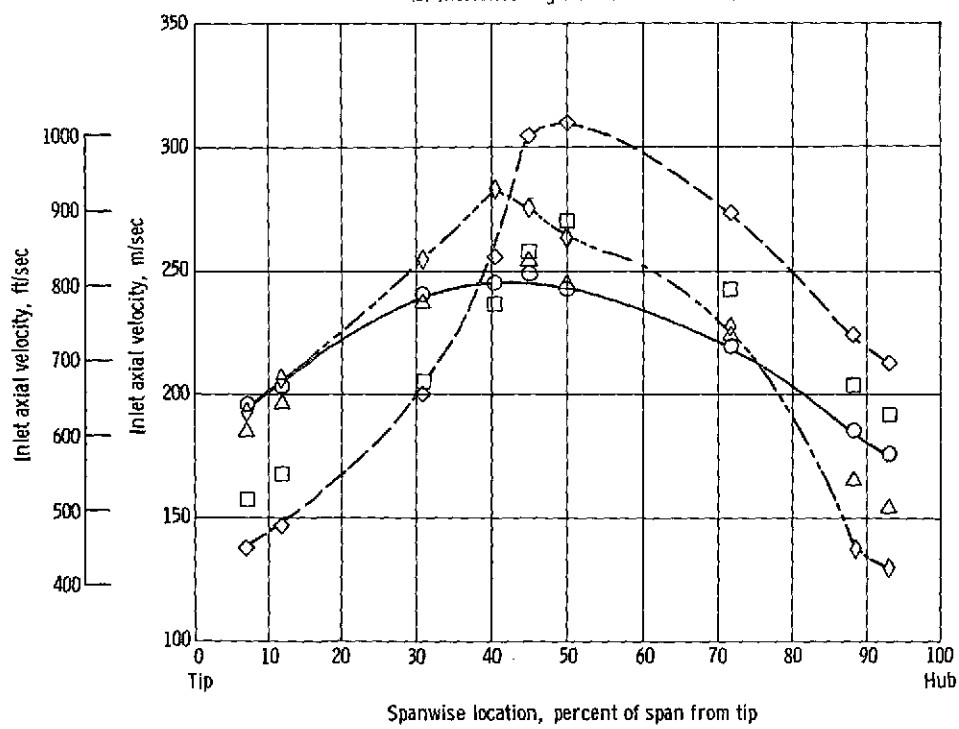

(c) Inlet axial velocity.

Figure 13. - Radial distributions of blade-element parameters at maximum flow with and without distortion (design speed).

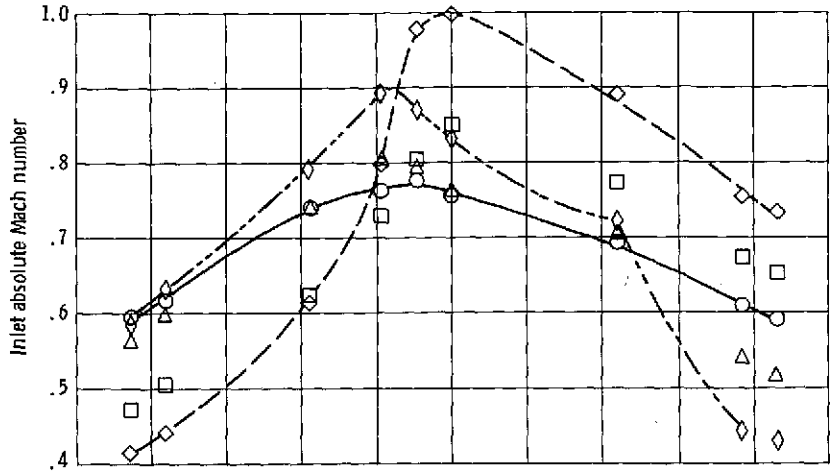

(d) Inlet absolute Mach number at blade leading edge.

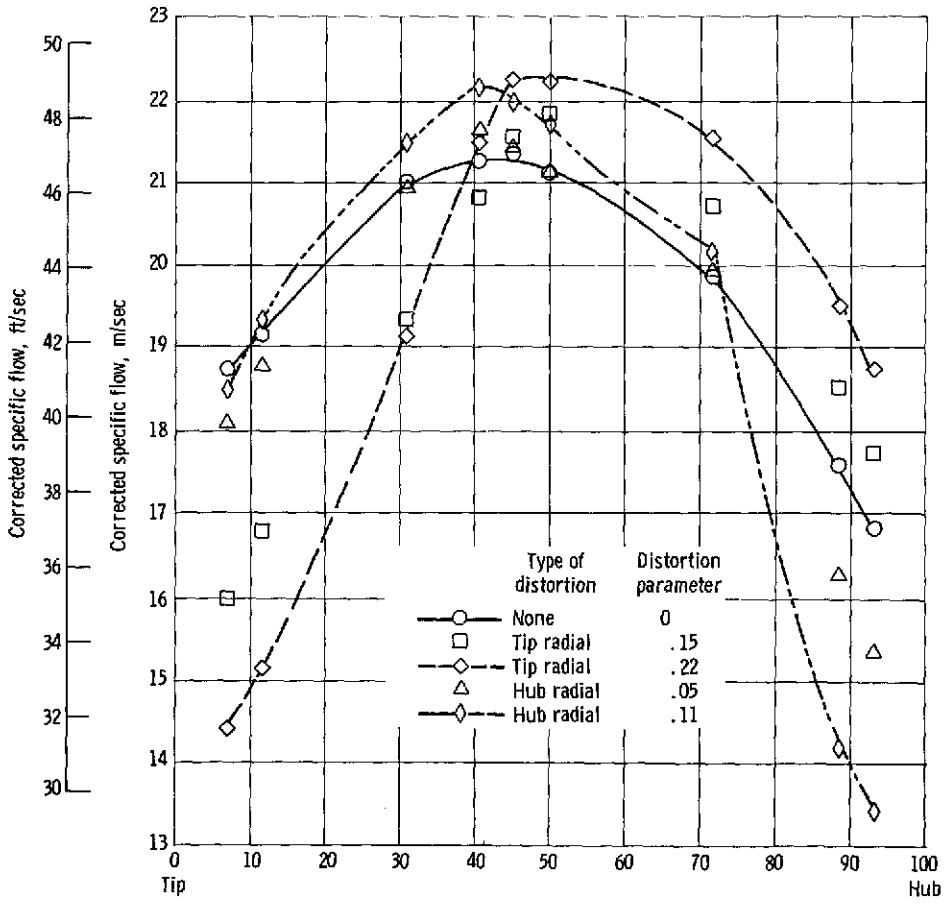

(e) Corrected specific flow at blade leading edge.

Figure 13. - Continued.

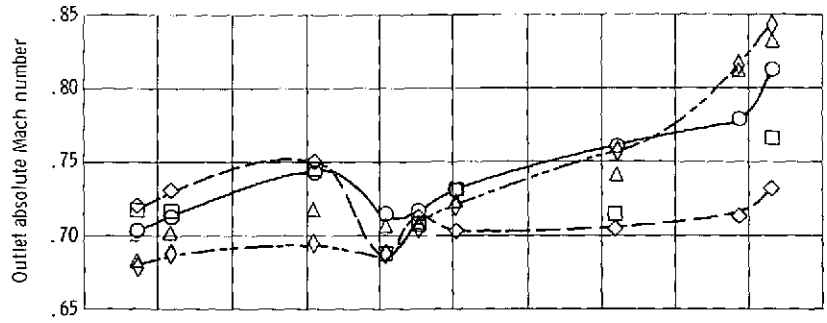

(f) Outlet absolute Mach number.

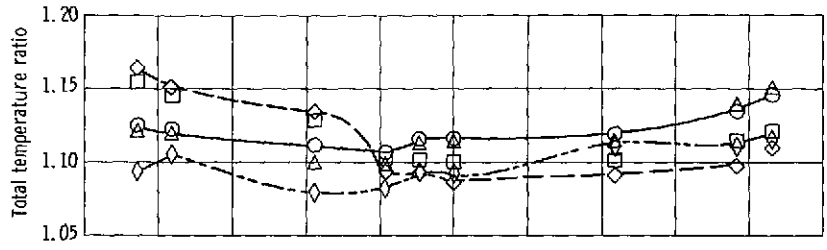

(g) Total temperature ratio.

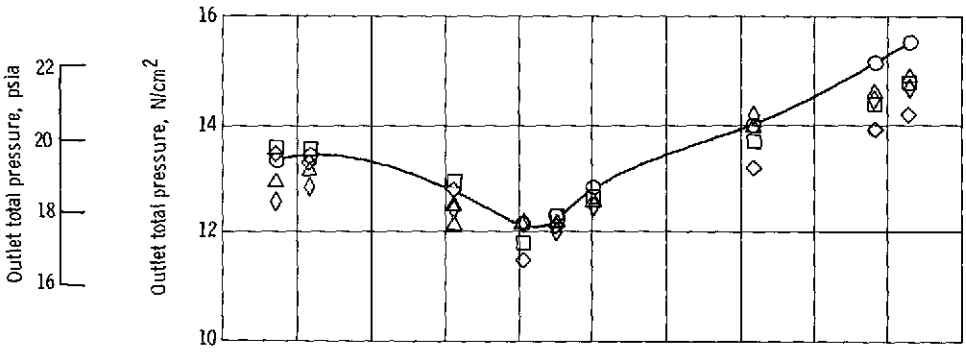

(h) Outlet total pressure.

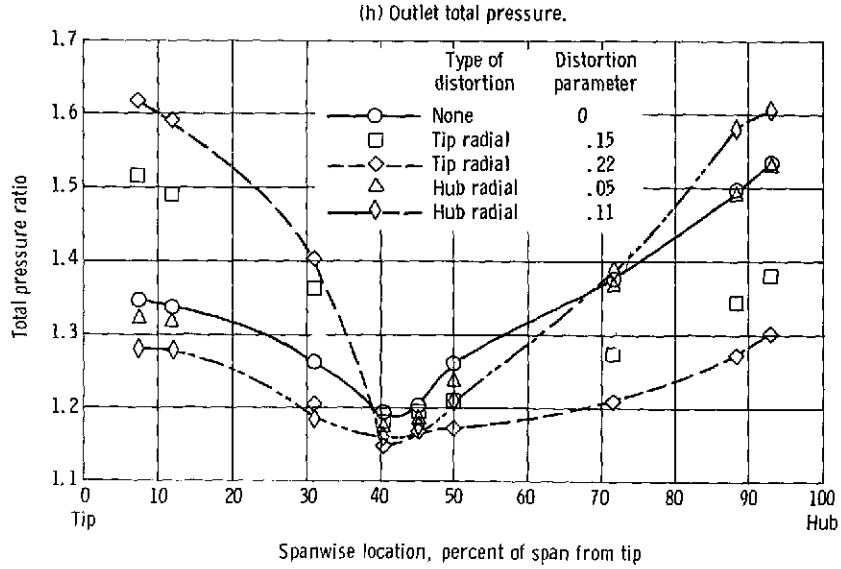

(i) Total pressure ratio.

Figure 13. - Continued.

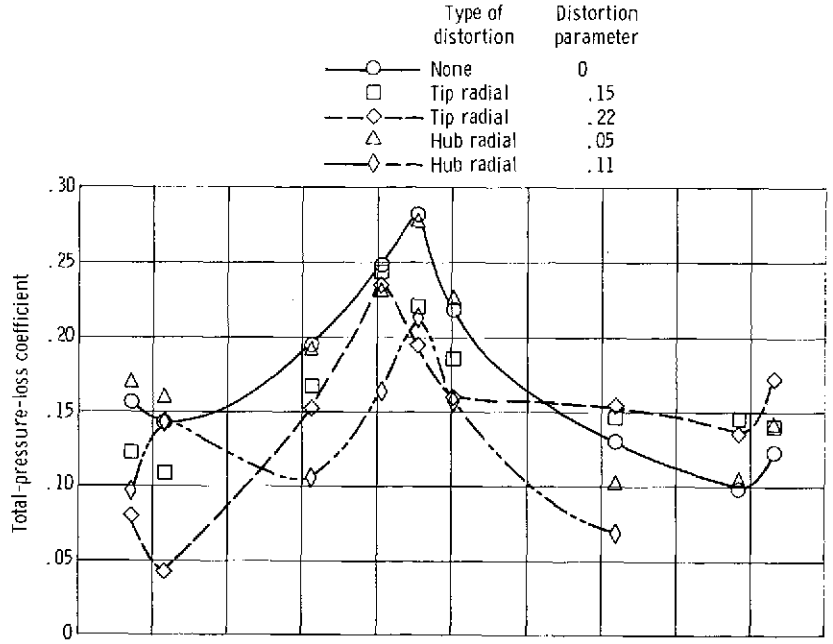

(j) Relative total-pressure-loss coefficient.

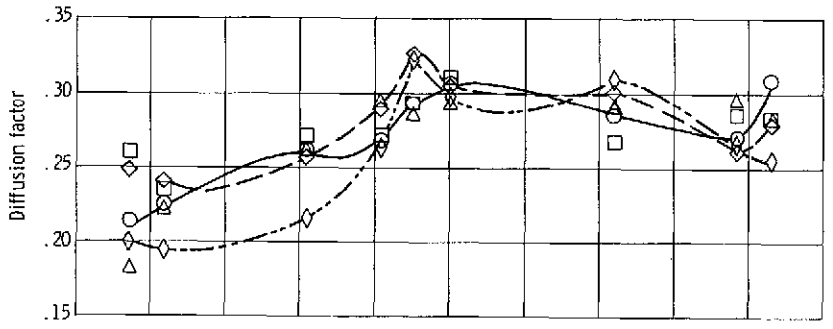

(k) Diffusion factor.

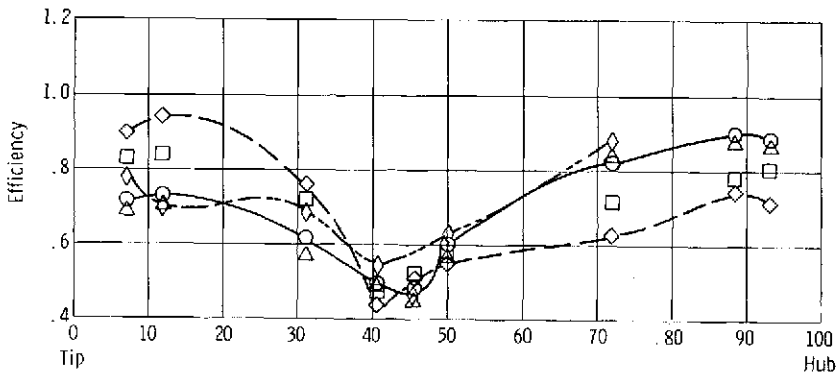

(l) Efficiency.

Figure 13. - Continued.

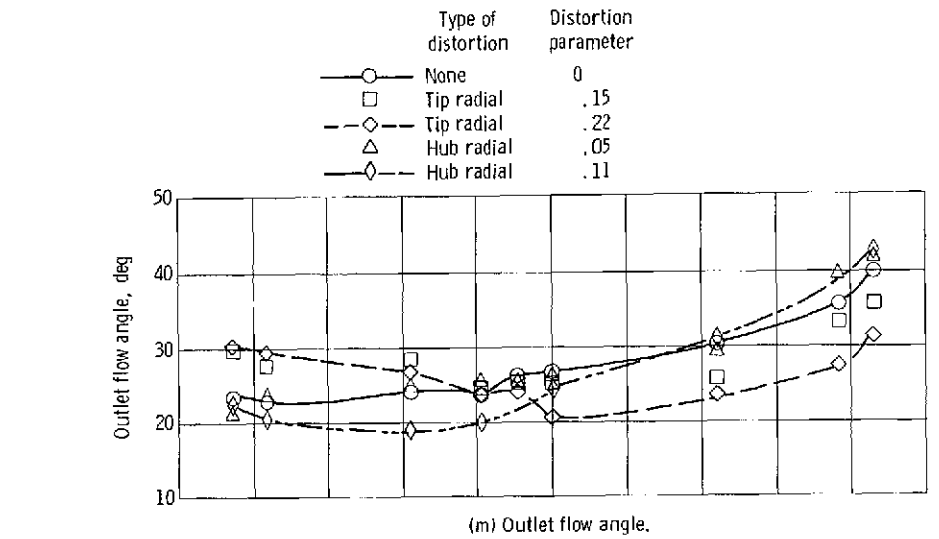

(m) Outlet flow angle.

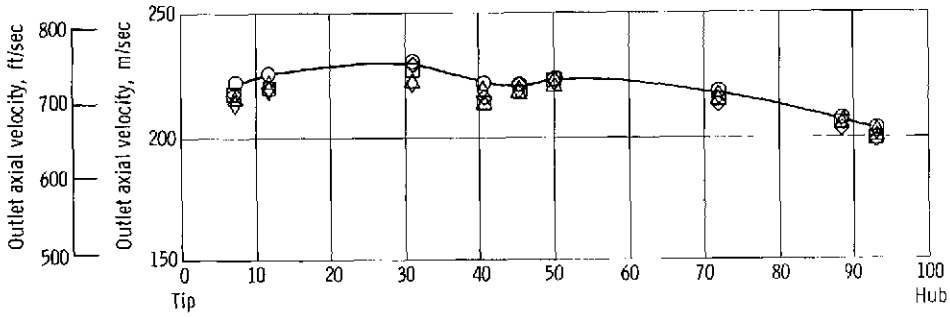

(n) Outlet axial velocity.

Figure 13. - Concluded.

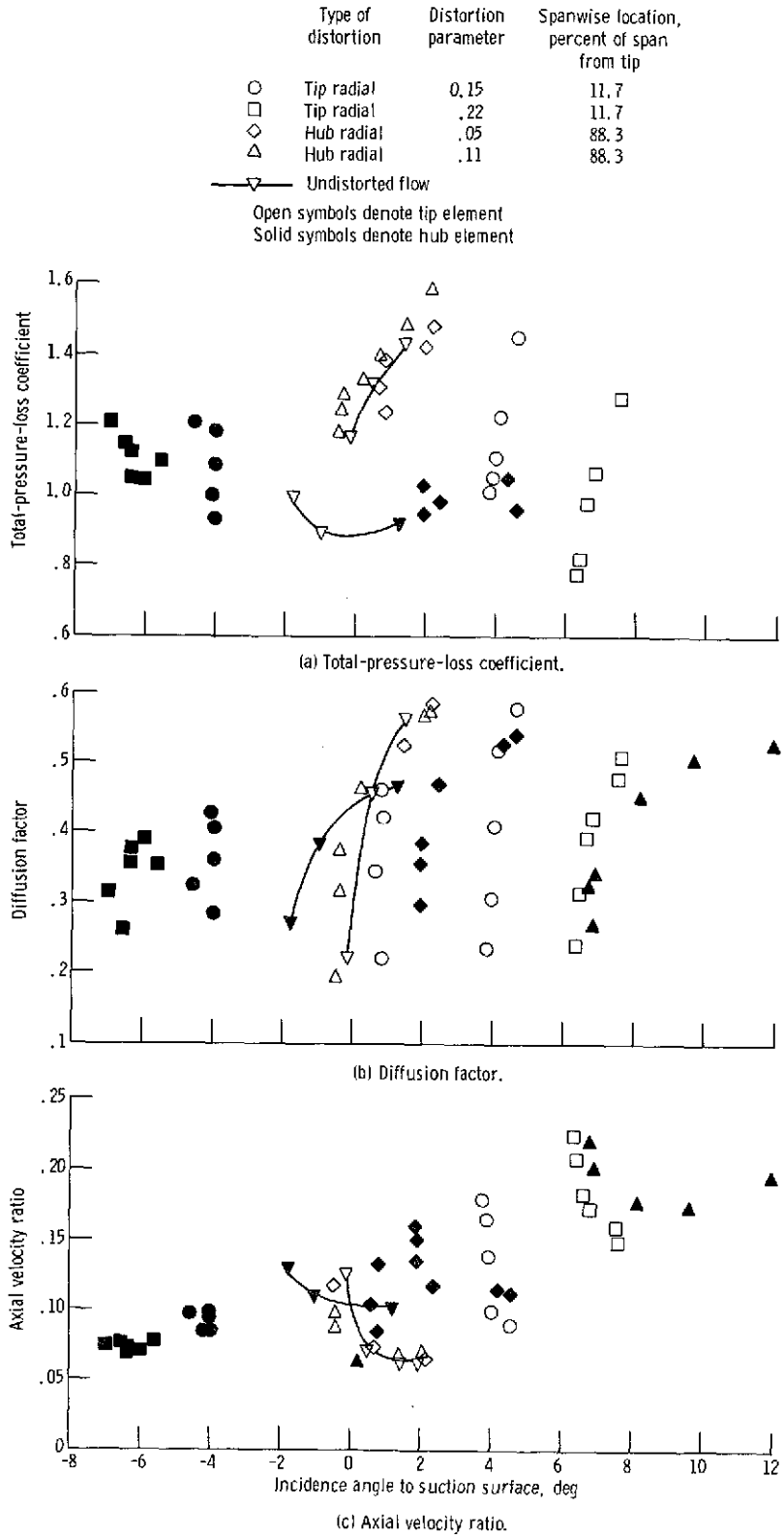

(a) Total-pressure-loss coefficient.

(b) Diffusion factor.

(c) Axial velocity ratio.

Figure 14. - Comparison of blade-element parameters with and without distortion - hub and tip elements at design speed.

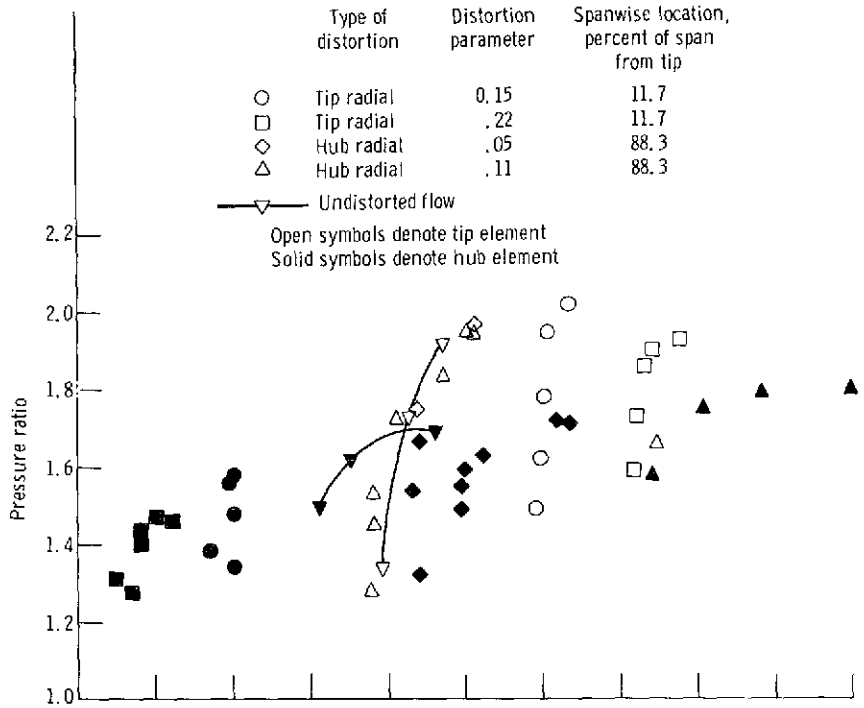

(d) Pressure ratio.

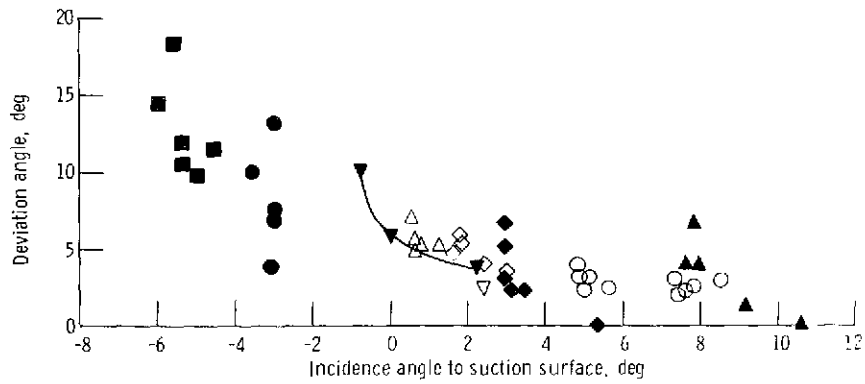

(e) Deviation angle.

Figure 14. - Concluded.

NASA-Langley, 1974 E-7545